Title
Understanding Kinesin's Gating Mechanism by Optical Trap

Author
Dogan, Merve Yusra

Publication Date
2013

Peer reviewed|Thesis/dissertation

Understanding Kinesin's Gating Mechanism by Optical Trap

By

Merve Yusra Dogan

A dissertation submitted in partial satisfaction of the

requirements for the degree of

Doctor of Philosophy

in

Engineering – Mechanical Engineering

in the

Graduate Division

of the

University of California, Berkeley

Committee in charge:

Professor Xiang Zhang, Chair
Professor Ahmet Yildiz
Professor Chris Dames
Professor Arunava Majumdar

Fall 2013

Abstract

Understanding Kinesin's Gating Mechanism by Optical Trap

by

Merve Yusra Dogan

Doctor of Philosophy in Engineering - Mechanical Engineering

University of California, Berkeley

Professor Xiang Zhang, Chair

Kinesin is a molecular motor that walks towards the plus end of microtubules by taking 8 nm steps in a hand over hand manner. The processive motility of kinesin requires its two motor domains (heads) to coordinate with each other. Interhead coordination involves a gating mechanism, where one of the heads cannot proceed until the other head goes through a certain act. Recent studies suggested that neck linker orientation is involved in coordination of the nucleotide binding and stepping motion of the two heads. In the leading head, the neck-linker is pointing backward, and inhibiting nucleotide binding. In the trailing head, the neck-linker is pointing forward, which allows the release of hydrolysis products and stepping towards the next tubulin binding site. To test this hypothesis, I used a novel optical trapping assay to directly measure microtubule release rate of the motor under a large range of constant forces. In the absence of nucleotide, the microtubule release increased as a function of force in both directions, with the release towards the plus-end was slightly faster than the minus-end under the same force. Addition of ATP resulted in faster release in both directions, consistent with nucleotide induced release properties of the kinesin motor. When kinesin was pulled from its linker in the forward direction, we observed faster release in the presence of ADP, which mimics the microtubule release. Remarkably, release was relatively slow when the linker was oriented in the backward direction by trap. Such asymmetry in the presence of ADP was not observed when kinesin was pulled from its head by a short DNA tether. These results suggest that geometrical constraints of the neck linker domains in a walking kinesin dimer break the symmetry of the two identical heads, such that the trailing head is free to move when the leading head is unable to bind nucleotide.

Dedicated to my children,
Osman Selim and Zeynep Duru

Table of Contents

List of Figures

List of Tables

Acknowledgements

During the many years I spent at Berkeley, I had the privilege of interacting with and befriending many people who have enriched my experience here, and whose company I truly treasure.

First comes my advisor Prof. Arun Majumdar who has introduced me to many research frontiers. He is an inspirational speaker and advisor with unmatched expertise and insight into several fields in science. I have been very lucky to be his student not only because he is a good scientist, but also because he has shown me great compassion and has shared my joy as I became a student parent. I know many women who have not been as lucky and I will always remain grateful.

Prof. Ahmet Yildiz has become my advisor in the last phase of my studies and I owe it to him to have completed my thesis. He has brought clarity to my research outlook when I was feeling highly confused in the route I had taken. I am forever indebted for his guidance and help.

I want to thank my collaborator Prof. Charles Craik whose constant curiosity I admire. He gave me the opportunity to do interdisciplinary research and I appreciate the exciting ideas that came up in our discussions.

During my studies in fluid mechanics, I have been especially impressed by Prof. Stephen Morris, and I want to thank him for patiently explaining difficult concepts and for his mentorship during my qualifying exams.

I also want to thank Prof. Xiang Zhang for becoming my thesis advisor, and Prof. Chris Dames for participating in my thesis committee.

I always remember my undergraduate advisor late Prof. Joseph 'Pepe' Humphrey with gratitude. He was the first one to introduce me to research and trust in my abilities. I really miss him.

I am grateful to many of my co-workers for acting as my student mentors and teaching me important skills. I admire their sharpness, and truly appreciate the insight they brought to my research and the patient support they provided throughout my career. Rohit Karnik has been the first to teach me in the lab, he introduced me to nanofluidics and microfabrication. Chuanhua Duan spent countless hours with me thinking through the difficult problems I encountered, acting as a true mentor. He also thought me microfabrication among many things. I appreciate his generous friendship. Andrey Revyakin introduced me to single molecule microscopy, and helped me take a new direction in my research. Mike Page helped me notice and resolve important subtleties in my work with peptides. Frank Cleary guided me through the project that is the subject of this thesis.

I have been involved with many research groups, and enjoyed the company of all the members. I want to thank Yang Zhao, Kedar Hippalgaonkar, Dusan Coso, Andy Zheng, Kenneth Castelino, Digvijay Raorane, Kaal Baheti, Ming-Chang Lu, Renkun Chen, Justyn Jaworski, Nihar Shah,

Pramod Reddy, Joe Feser, John Malen, Suzanne Singer, Gloria Chou, Keisuke Yokoyama who have been members of Majumdar group. Marta Cerruti, Renea Chu and Junyu Mai have become dear friends as well as coworkers, and I am thankful for their companionship. I am grateful to the welcoming members of Yildiz and Chu labs, Veysel Berk, Vedud Purde, Vlad Belyy, Yavuz Dagdas, Mark Dewitt, Jigar Bandaria, Tunc Yilmaz, Sheng-Min Shih and Kristin Schimert. They really helped me navigate through a field I have been a stranger to.

I shared many a laughter and tears with my friends whose support has been essential to my journey here. Elif Firat, Hatice Yildiz and Bilge Ozaydin have been my fellow student mothers who knew too well all my troubles, and whose conversation always brings me back to ease. Muna Guvenc has always been honest and spot-on with her observations, Nesrin Berk and Ayna Kochiyeva provided invaluable comfort and friendship, Zuleyha Sucu and Nihan Beyazoglu have lifted my spirits, Dahlia Halim has become my sister. I thank them and many others I am failing to mention for their friendship and prayers.

At every stage of my life, my family gifted me with a feeling of safety and unconditional love. My mother Meral Satoglu selflessly comes to my help at whim, without her I could not make it through. Words are never enough to thank her. My father Celalettin Satoglu is always protective and self-sacrificing; it is for him that I really wanted to complete this PhD. My sister Serife is my best and smartest friend who helps me see things clearly. I am blessed to have her. My brother Bugra is my best escape. He advises me to take it easy and I should listen to him more.

My parents-in-law Guler and Osman Dogan have accepted me as a daughter and come to my help in their sickness; I am greatly indebted to them.

My husband Hakan Dogan has endured all the hardship of my studies with me, maybe more than me. He has been my rock and I only wish I can become more like him. I am looking forward to the next phase of our life together.

My children Osman Selim and Zeynep Duru make me thank God every day. My life brightens with their little smiles and hugs. I hope I can become the mother they deserve.

I thank God for surrounding me with all these people and for getting me to finish my PhD.

Chapter 1. Background

1.1. The Cytoskeleton

The cytoskeleton is a network of filaments spanning across the cytoplasm that serves as the skeleton of eukaryotic and other cell types. This network determines a cell's shape, movement, physical strength and is responsible for functions such as organelle transport and pulling chromosomes apart during cell division [1]. It is composed of three different types of filaments with distinct properties and biological purposes (Figure 1.1). *Actin filaments* are the thinnest filaments at around 6nm in diameter. Their distribution beneath the cell cortex defines the cell surface shape. *Intermediate filaments* give the cell mechanical strength and function in conjunction with microtubules by supporting the tubulin structures. *Microtubules* are the thickest filaments at 25nm in diameter, and are mainly responsible for cargo transport and cell division [1].

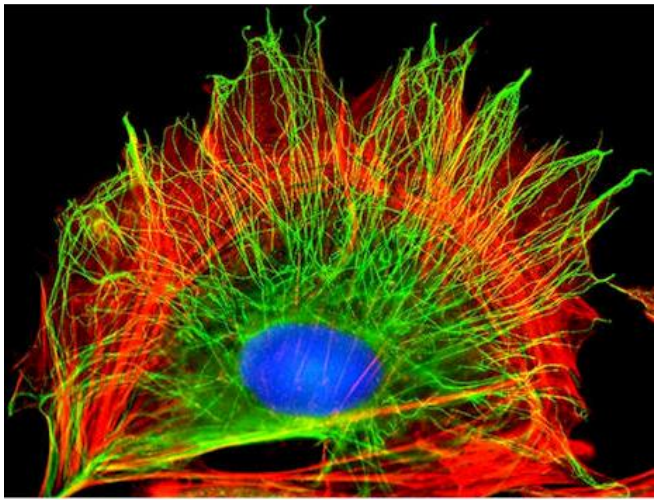

Figure 1.1. The cytoskeleton.
Image of a baby hamster kidney cell. DNA in the nucleus is stained blue, two of cytoskeletal elements are shown, microtubules (green) extending outwards from the nucleus and actin filaments (red) lining the cell surface. (Image by Albert Tousson)

1.1.1. Microtubules

Microtubules extend from the nucleus towards the cell surface. The unit elements of microtubules are polar α-β tubulin heterodimers that position themselves to form a 13 column hollow cylinder with outer and inner diameters of 25 and 12 nanometers and varying lengths that can reach 25 microns. Each column in this structure is called a protofilament (Figure 1.2).

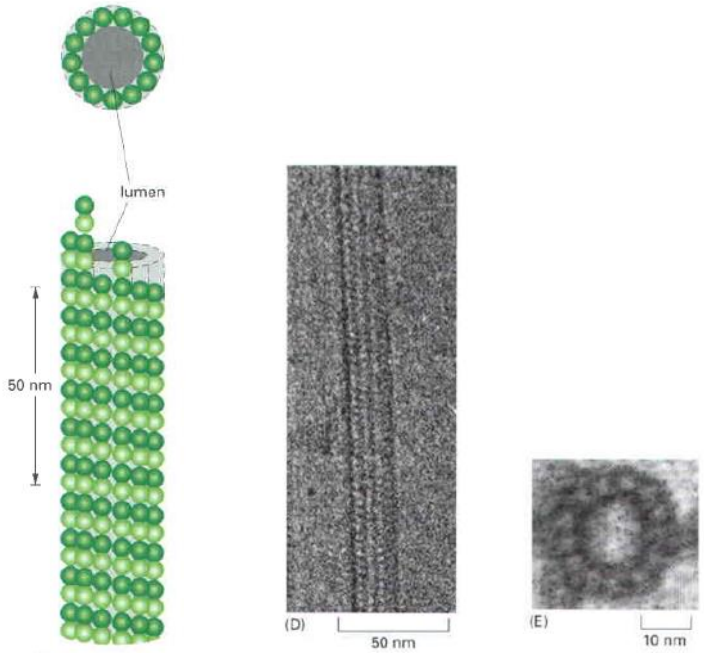

Figure 1.2. Microtubule Structure.
a) A microtubule is a hollow tube formed by 13 protofilaments. **b)** Electron micrograph of a microtubule segment (image from Richard Wade) **c)** Electron micrograph of a microtubule cross-section (image from Richard Linck). (Figure reproduced from [1])

Since the tubulin heterodimers line up in the same configuration, the polarity is preserved throughout the microtubule, with α-tubulin exposed end being (-) and β-tubulin exposed end being (+) charged. This polarity is vital for microtubule functions. The structure of the tubulin heterodimers is shown in Figure 1.2. α- and- β-tubulins are two globular proteins that are strongly but noncovalently bound to each other. Microtubule polymerization is a GTP driven process. The dynamics at the β- end determine microtubule growth or depolymerization. If the rate of the hydrolysis is higher than tubulin addition, the microtubule starts a rapid dissociation. This dynamic instability is regulated in the cell to control microtubule elongation or shortening in order to assist in different cell functions such as splitting sister chromosomes during mitosis [1].

1.2. Molecular Motors

Organelle transport inside the cell heavily depends on the cytoskeleton. It serves as the highway along which proteins carry cargo to various cell sites. A special class of proteins called *cytoskeletal molecular motors* walk along filaments by hydrolyzing ATP (Figure 1.3) and using the resulting energy to take a step in their preferred direction. They all have a motor domain, referred to as the 'head', with which they hydrolyze ATP and bind the filaments, and a cargo carrying domain, referred to as the 'tail'. *Kinesin* and *Dynein* are two such molecular motors that walk along the microtubules and *Myosins* are the motors that walk on actin filaments [1].

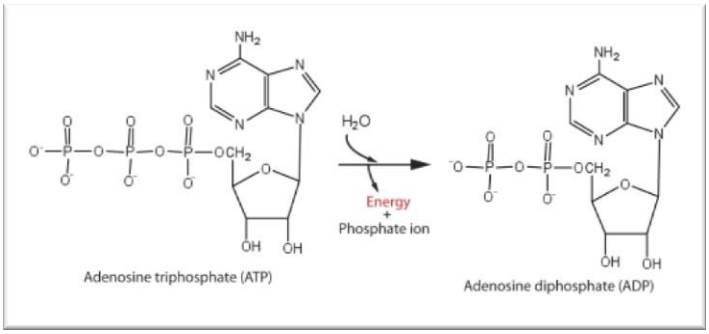

Figure 1.3. ATP Hydrolysis.
General equation for ATP hydrolysis: $ATP + H_2O \rightarrow ADP + P_i + 7.4$ kcal/mol
P_i is the symbol for the inorganic phosphate anions $H_2PO_4^-$ and HPO_4^{2-}.
A single ATP hydrolysis generates 100 pN·nm of energy, equivalent to 24 kT.

Myosin superfamily comprises above twenty different classes of proteins, which share common properties of actin binding and ATP hydrolysis. Myosins V and VI are the myosin motors that take successive steps along the actin filament and transport cargo. Myosin V (Figure 1.4a) walks towards the (+) end of actin and Myosin VI towards the (-) end [2,3].

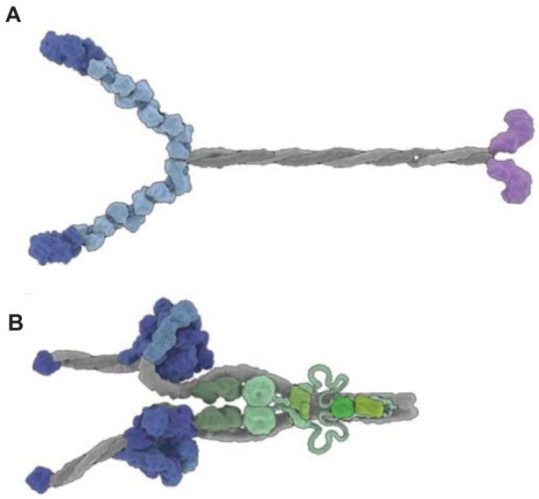

Figure 1.4. Representative structures of cytoplasmic motor proteins.
a) Myosin V is a dimeric protein that walks along actin filaments. Its structure is composed of a *motor domain* (dark blue) that hydrolyses ATP, *lever arms* (blue) as motile elements consisting of light chains, *coiled coil* domain (grey) and *tails* (purple) that bind cargo. **b)** Cytoplasmic dynein walks towards the (-) end of the microtubule. Its components include *microtubule binding domains* (dark blue) at the end of a *coiled coil stalk* (grey) that connects to the six AAA+ ATPase *motor domains* (dark blue) where ATP hydrolysis takes place. The motile element is the *linker* (light blue) that spans across the ATPase rings of the motor domain. Cargo binding occurs at the *intermediate and light chains* (different shades of green) (Dynein figure by Janet Iwasa) (Figure adopted from [4])

Dyneins move towards the (-) end of the microtubules, which is typically towards the cell center. Dynein family of motors is divided into two categories as cytoplasmic and axonemal

dyneins. Cytoplasmic dynein (Figure 1.4b) is found in almost all eukaryotic cells. It moves processively along the microtubule, and transports vesicles to specific destinations. It is also responsible for localizing the Golgi apparatus inside the cell and for moving the chromosomes during cell division [1]. Axonemal dynein is only found in flagella and cilia and aids movement by sliding the microtubules in the axonemes.

1.2.1. Kinesin Superfamily

The fourteen families in the kinesin superfamily contribute to numerous processes in the cell, including vesicle and organelle transport, mitosis and meiosis. All kinesins share a common motor domain of 340-350 amino acids [5], but vary in the rest of their structures and properties(Figure 1.5). Kinesin-1, namely the conventional kinesin, processively walks towards the (+) end of the microtubule, from the cell center to cell periphery. There is however kinesins that walk towards the (-) end (Kinesin-14 class) or don't show any directional preference and destabilize microtubules at ends (Kinesin-13 class). The different structures of the kinesins make them useful for different tasks. For example, kinesins 1, 2 and 3 transport vesicles, whereas kinesins 4 and 10 work in chromosome positioning [6].

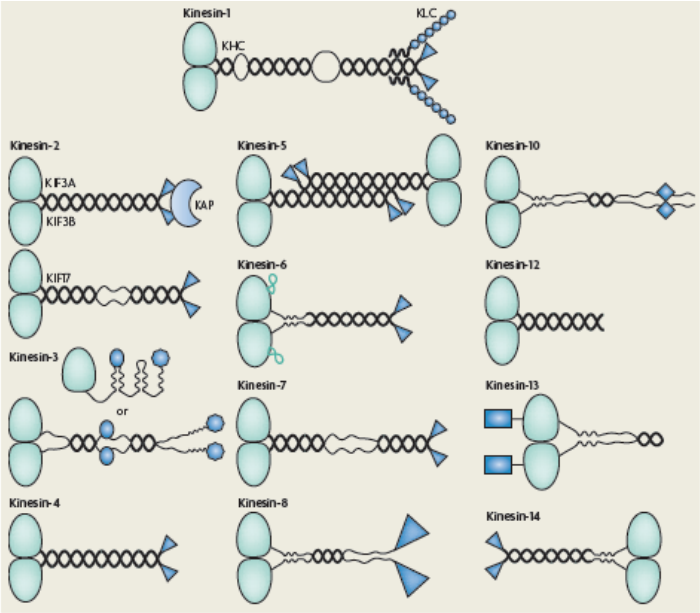

Figure 1.5. Kinesin Superfamily.
Structures of the 14 families of kinesin are shown. All of them have a motor domain (light green). The position of the motor domain determines the direction of motility. Most kinesins have coiled coil regions (dark green). The unique regions in the structure differ according to the different functions and properties of kinesins. (Figure modified from [6])

1.3. Structure of Kinesin

The kinesin structure is a double heavy polypeptide chain that forms a homodimer and binds two light chains. Each heavy chain can be divided into several regions according to their shapes and purposes. These will be described as the regions of head, neck linker, tail and the stalk. The stalks spiral around each other to form a coiled coil that can be further divided into domains of two coiled coils and a neck coiled coil connected by two hinges (Figure 1.6).

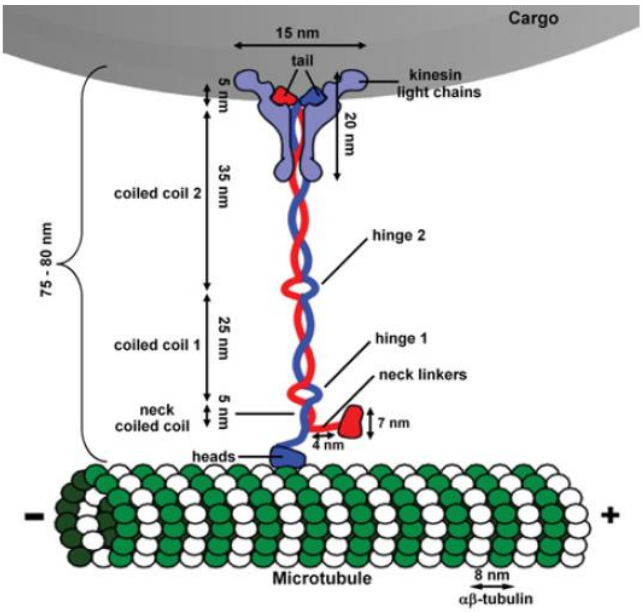

Figure 1.6. Kinesin structure.
A schematic of a microtubule-bound kinesin carrying cargo. Different parts of the structure and relevant dimensions are labelled. (Figure from [7])

1.3.1. Head

The head region, also known as the 'motor domain' is the site for both microtubule binding and ATP hydrolysis. 7.5 nm x 4.5 nm x 4.5 nm in size, it is composed of 325 amino acids that form a central seven-stranded β-sheet with three α-helices on both sides [8,9].

Figure 1.7 shows the structure of the motor domain, where β-strands are colored light blue and the α-helices are colored pink. Green regions are the microtubule binding sites, and purple regions are nucleotide binding sites. A representation of a bound ADP is also shown with base and ribose colored orange and phosphates colored yellow [10].

This crystallography image reveals that the two heads of the kinesin cannot simultaneously bind the microtubule in the same configuration. The nucleotide state determines how tightly the

head binds the microtubule. In ATP state for example, when bound to the microtubules, the motor domain attains an immobilized and rigid conformation [11].

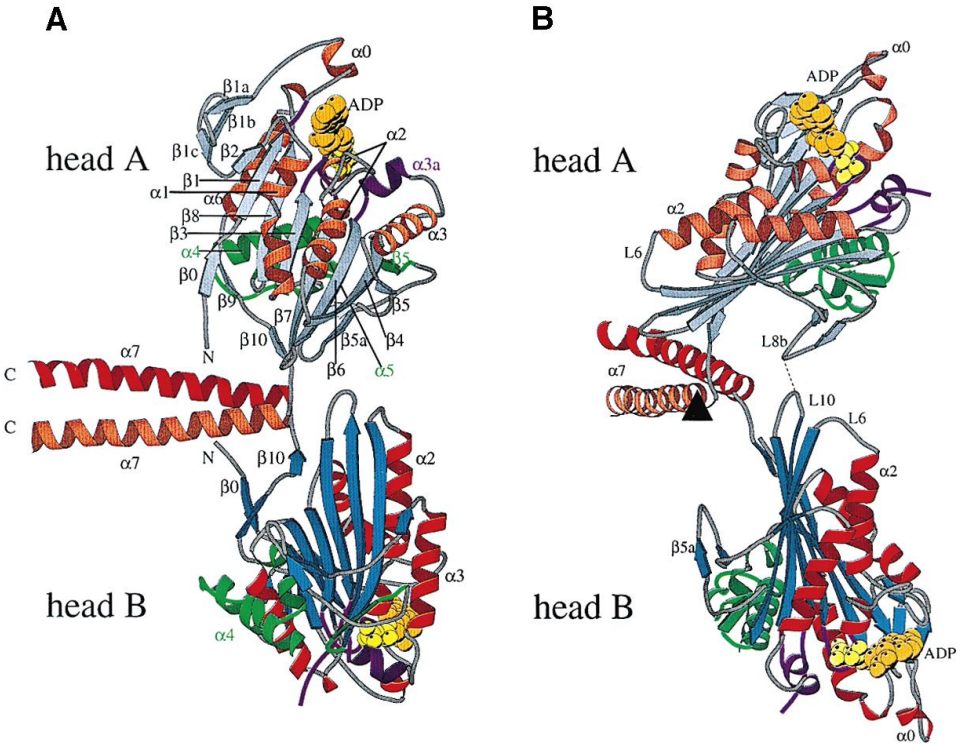

Figure 1.7. Motor domain of kinesin.
In this crystallography image of kinesin motor domain, β-strands are colored light blue and the α-helices are colored pink. Microtubule binding sites are shown green, nucleotide binding sites are shown purple. ADP is also represented, where base and ribose are colored orange, and phosphates are colored yellow. (Figure from [10])

1.3.2. Neck linker

The neck linker consists of about 15 amino acids, and stretches between the motor domain and the first coiled coil of the stalk [12]. It provides communication between the two motor domains via internal strain and determines the directionality of the kinesin movement [7,13]. The conformation of the neck linker is decided by nucleotide binding. In the absence of nucleotides or ADP binding, the neck linker remains flexible. Upon ATP binding, however, it becomes rigid in an extended position, called a 'docked' state [14].

Figure 1.8 shows the docked (ATP) and undocked (ADP) states of the neck linker. A region of the motor domain (grey) called the switch-2 cluster (green) contains most of the microtubule binding surface. In ADP bound state, the switch-2 cluster blocks the neck linker from entering the core of the motor domain. In Figure 1.8a, the neck linker is thus invisible. When kinesin is bound to the microtubules and is in an ATP state, the switch-2 cluster positions itself such that

a groove opens up and the neck linker can dock into the core of the motor domain. Here the neck linker is shown in blue.

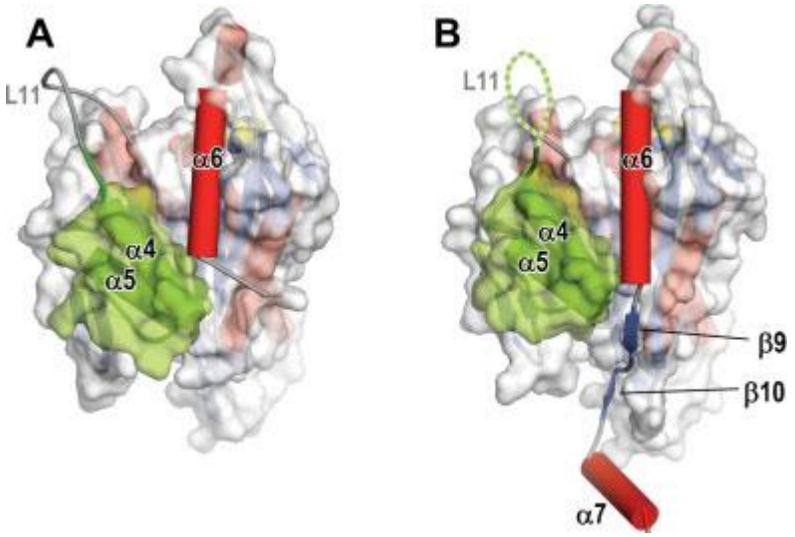

Figure 1.8. Neck linker docking and undocking.
a) In ADP state, switch-2 cluster (green) blocks the neck linker from binding the core domain (grey). **b)** In ATP state, switch-2 cluster moves and the neck linker (blue) can enter into the binding grove. (Figure from [12])

1.3.3. Tail

The tail is where kinesin binds its cargo. This is a globular domain that binds membranous organelles on its own, and attaches light chains to selectively bind different kinds of cargo via adapter proteins [15]. It has been shown that the tail interacts with the head and inhibits it in the absence of cargo [16–18]. In solution the head and tail are attached to each other. In this configuration, kinesin is bent in its stalk region, and while it is able to bind microtubules, it remains immotile. When a cargo finds and binds an active kinesin, the tail and head will detach and the stalk region will unfold. This mechanism allows kinesins to pause without a cargo and consume energy when they are bound to their respective cargo [18,19].

1.3.4. Stalk

The two coiled coils of the stalk are rigid α-helix regions that do not have conformational flexibility [20]. Located between these two regions is the hinge-2, also known as the 'kink'. This is a very flexible section where the stalk folds for kinesin to enter its inactive state. Hinge-1 connects coiled coil 1 to the neck coiled coil. This region is essential for the coordination of several motors with each other while carrying a single cargo [21,22]. The neck coiled coil induces the dimerization of the kinesin heavy chains. This region is thought to be important for

regulatory purposes rather than for motility, since its substitution does not affect force generation or maximum velocity [23].

1.4. Mechanism of Kinesin Motility

1.4.1. Kinesin Processivity

Conventional kinesin is an ATP-driven motor with an 8-nm step size. Kinesin has processive motility, meaning that it can take several steps along the microtubule before dissociating from its track. Kinesin processivity was first demonstrated by Howard et al. with a gliding assay where microtubules moved on single kinesin motors bound to a glass surface [24]. Consequently, Block et al. observed single kinesins attached to glass beads moving about a micron along the microtubule without dissociating [25].

Since the motor hydrolyzes one ATP for each step, the number of steps the motor takes should correspond to the number of ATP molecules hydrolyzed while the motor is bound to the microtubule [19]. Hackney et al. therefore defined processivity as the ratio of ATP molecules hydrolyzed per microtubule binding event by a motor [26]. Motors with a ratio greater than one are called processive, and less than one are called nonprocessive. The average ratio for kinesin is about 125, showing that kinesin is a highly processive motor [27].

Kinesins with two heads show processive motility, whereas single headed mutants are nonprocessive [28,29]. Processive kinesins are also seen to be walking along a single or two protofilaments of the microtubule, whereas nonprocessive motors that are released from the microtubule after one step, seem to change their protofilaments as expected from a diffusive movement [27,28,30].

1.4.2. Kinesin Walking Mechanism

Kinesin walks along the microtubule in a hand-over-hand manner [31]. When both its heads are bound to the microtubule, the rear head is 8-nm behind the front head. By taking a 16-nm step forward, the rear head becomes the leading head and the center of mass of kinesin moves by 8-nm (Figure 1.9). This process is powered by ATP hydrolysis (Figure 1.3).

In the first snapshot shown in Figure 1.9, both heads of kinesin are strongly bound to the microtubule; the front head (green) has no nucleotide and the rear head (blue) has an ATP. The neck linkers are positioned such that the neck linker of one head is pointing towards the other head. Strong bindings of both heads generate strain on the neck linkers, which further causes the rear head to rapidly hydrolyze ATP to ADP-Pi and prevents the front head from binding ATP [13,32].

After the rear head hydrolyzes ATP, it enters a weakly bound ADP state. Once the rear head is in this weak binding state, the front head can bind ATP [13].

Binding of ATP by the front head causes a conformational change of its neck linker, called 'neck linker docking' where the neck linker will fold over and dock towards the forward direction [11]. This movement causes the rear head to be thrown forward and after a short diffusional search, to bind to the next available spot on the microtubule, release its ADP and become the leading head [33](Figure 1.10). The same cycle repeats with kinesin position 8 nm ahead of the first snapshot.

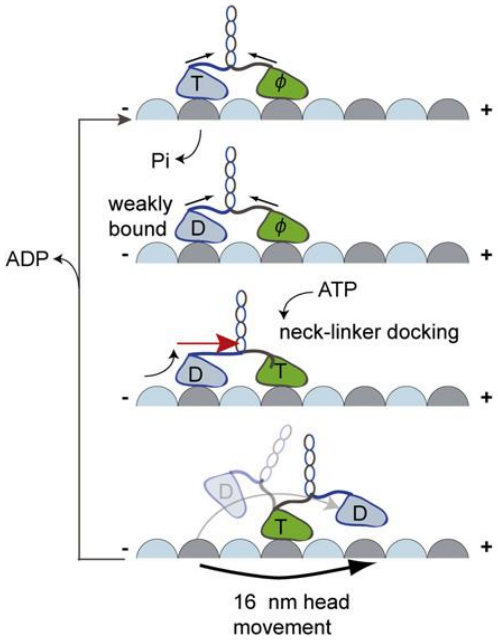

Figure 1.9. Hand-over-hand walking model.
The rear head of kinesin steps in front of the other head, and becomes the leading head by taking a 16 nm step forward, and moving the kinesin center of mass by 8 nm. [Representations: ATP (T), ADP (D), no nucleotide (ϕ)] (Figure from [34])

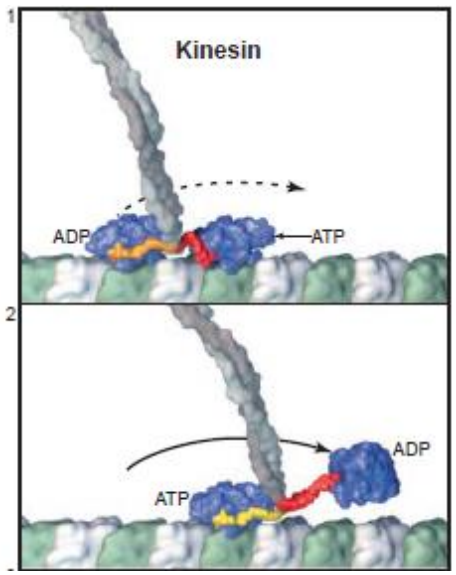

Figure 1.10. Kinesin's step.
Neck linker of the front head is shown red in the first picture. Once it is docked as depicted yellow in the second picture, the rear head gets thrown forward. (Figure modified from [33])

1.4.2.1. The Asymmetric Hand-Over-Hand Model

Kinesin dimer is a symmetric structure and the microtubules are helically symmetric. However, kinesin loses its mirror symmetry when the heads are bound to a microtubule, because both heads need to orient in the same direction matching the symmetry of the microtubule lattice [13,35–39]. As a consequence, both heads become unique and their stepping behavior is not identical either. The accurate model of walking is therefore an asymmetric hand-over-hand model [31,40–46].

In this model, the step of the trailing head alters according to which head takes this role. One of the heads steps forward from the left side of the microtubule, twisting the neck linker, and the other one steps forward from the right, untwisting it (Figure 1.11). This prevents the curling of the stalk and the rotation of cargo at every step. The two steps also differ as fast and slow since it is easier to step when the linker is not twisted and harder when twisted. This cycle returns to the exact same pattern after every other step [41,47,48].

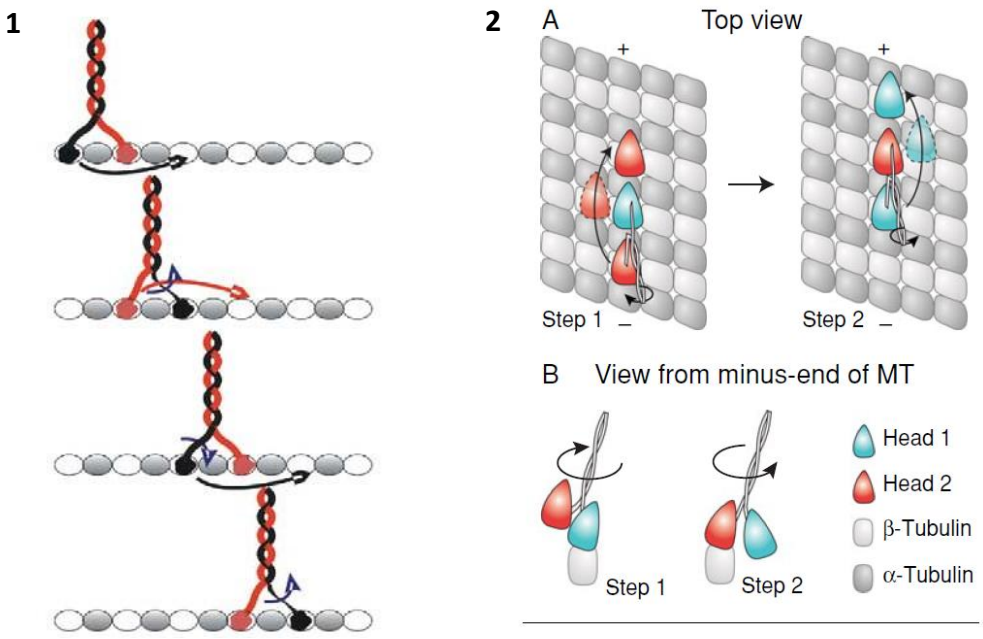

Figure 1.11. Asymmetric hand-over-hand walking mechanism.
1) The two heads are not identical in their step. One of them goes forward from the left side of the protein, whereas the other one goes from right. Their alternating steps cause twisting and untwisting of the neck linker with every second step. (Figure from [48]) **2A)** Top view showing the two heads stepping from different directions. **2B)** View from minus-end of the microtubule showing the twisting and untwisting of the linker. (Figure from [46])

1.4.2.2. Backward Stepping of Kinesin

It is known that a kinesin head goes into a diffusional search between steps before it finds the next available stop for binding on the microtubule. Carter and Cross have shown that applying a force on kinesin can influence the direction of its step, and make it take successive backwards steps [49]. According to this study, pulling backwards on kinesin with increasing load decreases its probability to step forward and doesn't change the probability of stepping backwards. At a stall force of 7.2 pN however, the probability of stepping forward or backward becomes the same. Applying higher forces reverses the direction of kinesin stepping and at this point kinesin essentially walks backwards (Figure 1.12) [49–51]. This is an important study demonstrating backward stepping of kinesin. However, it is not sufficient to understand the properties of kinesin head release from the microtubule, since the applied force here is shared between the two heads. Determination of kinesin head release rate at a constant force necessitates a more elaborate assay as will be discussed in the next chapter.

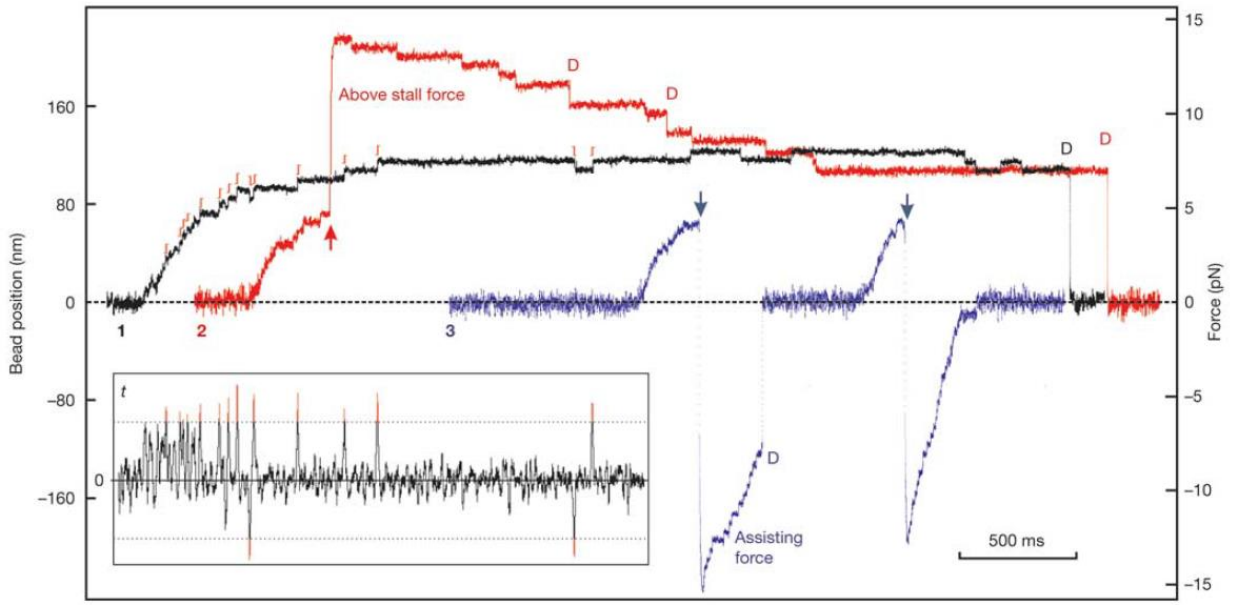

Figure 1.12. Backward stepping of kinesin.
Optical trapping traces showing single kinesins **1)** stepping forward under backwards load smaller than stall force (black) **2)** starting to walk backwards upon sudden application of backward force above stall force (red) **3)** advancing forward upon application of sudden assisting load (blue). (Figure from [49])

1.5. Models for Coordination between Heads and Gating

All the stages of kinesin stepping require the two heads to coordinate with each other perfectly in order for kinesin to advance long distances without dissociating from the microtubule. During the stepping cycle, there are intermediate states, where one of the heads cannot proceed until the other head goes through a certain act. In other words, one head needs to wait until the other one opens the gate. Several gating mechanisms have been proposed to explain how one head can influence the actions of the other. These are not necessarily mutually exclusive, and there may be more than one mechanism at work [52,53]. The role of the neck linker is especially highlighted in most of these theories.

Gating can be mediated by intramolecular tension, nucleotide binding or by the structure of a two head bound state of the motor, all of which involve the neck-linker domain [53]. These gatekeepers can regulate important aspects of stepping such as microtubule attachment and detachment of kinesin (‘polymer gating’), or a process in the ATPase cycle (‘nucleotide gating’). One of the two cases that involves polymer gating is based on a model where between the steps, one head is bound to the microtubule while the second one is parked against it making a one-headbound intermediate [54]. The second head is unable to bind to the microtubule until the first head binds ATP. Hence, the gatekeeper here is ATP binding (Figure 1.13a).

All the other gating mechanisms assume that both heads are bound to the microtubule. They call this kind of coordination 'action-at-a distance'. All these theories involve the neck linker and have different hypotheses for its role and function.

The second case of a possible polymer gating mechanism suggests that microtubule detachment of kinesin is dependent on the internal tension between the heads. When both heads are bound to the microtubule, a rearward tension is built up on the front head due to its neck linker extending backwards, and similarly, a forward tension is built up on the rear head because its neck linker extends forward (Figure 1.13b). One proposed gating mechanism states that tension on the rear head decreases its microtubule affinity and accelerates its detachment from the microtubule[28]. Here, tension is the gate keeper for microtubule detachment of the rear head. Supporting experiments have shown that less force is needed to detach a kinesin monomer from the microtubule if pulling forward as opposed to pulling backwards regardless of nucleotide state [55]. It is therefore expected that the rear head, and not the front head, will detach. The role of neck linker tension has been studied by comparing kinesins with extended linkers to wildtype kinesin [34]. In the absence of any external load, modified kinesins slow down in their tracks due to futile cycles of ATP hydrolysis that do not lead to a mechanical step. However, they recover their speed once a load is applied with an optical trap, i.e. once neck linker tension is restored. Load driven kinesin remains processive even in the absence of nucleotides. It is also considered that the neck linker docking in the front head can cause increased tension on the rear head, hence contributing to accelerated detachment of the rear head in such a gating mechanism.

A different way in which the tension in the neck linker can act as a gate is by regulating nucleotide binding and release (Figure 1.13c). Here, nucleotide gating could take place in the rear or front head. The studies supporting rear head gating were first done by Hackney [42] who showed that the one head can release an ADP once, but before it can release another ADP, it needs to wait until the front head binds ATP. It is believed that ATP binding initiates neck linker docking, and the tension in the neck linker prevents ADP release. This idea of gating is also supported by the results of Uemura and Ishiwata [56] who found that affinity of ADP for kinesin increases with forward external load, and decreases with backward load.

Alternatively, a front head nucleotide gating mechanism was first introduced by Rosenfeld et al. where they claimed that the main role of internal tension was to block ATP from binding to the front head to ensure that the heads remain out of phase [13]. By keeping the front head in a tightly bound state, this model also explains the likelihood of rear head detachment. Klumpp et al. further state that the rear head detachment is the step that allows ATP binding to the front head [35]. In other words, once tension is relieved from the front head, ATP can bind. Another supporting study was done by Guydosh and Block where they used a non-hydrolysable ATP analog and saw that the heads must first take a rearward step to release it (the ATP analog could only be released from the rear head) and bind ATP in order to return to their regular motion [57]. This has increased confidence in tension as the gatekeeper for ATP binding and the stepping of the front head.

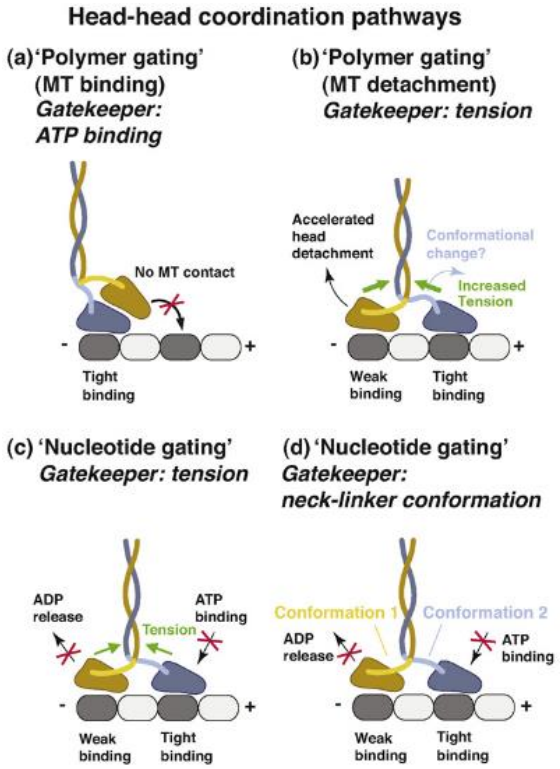

Figure 1.13. Possible gating mechanisms.
Different possibilities for head-head coordination: **a)** Microtubule binding may be regulated by ATP binding. **b)** Microtubule detachment may be regulated by intermolecular tension. **c)** Nucleotide binding and release may depend on tension **d)** or neck-linker conformation. (Figure from [53])

The neck linker may have a more active role in the stepping mechanism, as opposed to its passive role of just providing tension. It is plausible that the neck linker may actually adopt different conformations in its backward or forward stretched positions that allow it to interact allosterically with the catalytic core, where it can block ATP binding or ADP release (Figure 1.13d). Evidence for this idea comes from Clancy et al. whose experiments demonstrate that in addition to tension, neck linker docking is also responsible for gating [58]. They examine the gating mechanism with kinesin mutants with lengthened neck linkers, and see that gating is still in place. By looking at the consequence and duration of events, they conclude that the reorientation of the neck linker is responsible for gating as opposed to intermolecular tension. Their results are consistent with Toprak et al.'s results showing that for ATP binding by the front head, neck-linkers need to be separated but it is not necessary for both heads to strongly bind the microtubule[59]. Guydosh et al.'s findings support this idea as well by stating that before ATP binding, the ADP-bound head is unbound to the microtubule [60].

Besides these gating mechanisms, it is also possible that the microtubule itself interacts with kinesin in such a way that it plays a role in the regulation of nucleotide binding. This has been implied by the findings that the microtubule structure changes upon kinesin binding [61]. Recently, Kikkawa [62], and Sindelar and Downing [63] have used cryoelectron microscopy to

resolve the structural changes upon microtubule attachment of kinesin. Based on these models, Sindelar and Downing propose a seesaw mechanism where microtubules activate the ATP-sensing mechanism of kinesin [63,64]. According to this model, microtubule attachment happens with a direct contact with the switch II helix and this contact region acts as a pivot point around which kinesin head tilts. Upon ATP binding, the switch loops inside the motor domain tilt the kinesin head resulting in neck linker docking and a power stroke that translates cargo.

1.6. Objective of This Study

As discussed above, resolving the role of neck linker in the kinesin walking mechanism is essential to understand how kinesin operates.

In an instant when both the kinesin heads are bound to the microtubule, the rear head is in an on-state, meaning it can bind ATP, while the front head is in an off-state and cannot bind ATP (first snapshot of Figure 1.9). To investigate the reason for this phenomenon, one needs to carefully identify the differences between the states of these two heads. Important differences between them can be listed as: *First*, they are not structurally symmetric when bound on the microtubule. *Second*, their neck linkers are not symmetric. One of them may be twisted inwards while the other one is unwound. *Third*, the orientation of the linkers and the tension on them is not the same. In regard of these differences, it is unclear whether ATP binding depends on these structural and geometrical differences, or whether the tension on the neck linker regulates nucleotide binding via a gating mechanism.

All these differences necessitate that a study to understand the on and off-states of kinesin, mimics both states appropriately. With this in mind, we want to look at kinesin monomers as opposed to dimers, so we will have the ability to manipulate and know which state we are dealing with. A monomer being pulled forward will represent the rear head and a monomer being pulled rearward will represent the front head (Figure 1.14).

Using kinesin monomers, our objective in this study is to firstly answer the question of whether the orientation of the neck linker plays a role in gating the ATP binding. If so, to what degree? We aim to answer this by applying a known tension on the neck linker in both directions and looking at kinesin release from the microtubule under different nucleotide conditions. Comparing these results to cases where the neck linker is free without any tension will help clarify the function of neck linker in gating.

An intermediate goal of our study is to determine if there is an asymmetry in the microtubule binding domain, and whether such an asymmetry can be nucleotide dependent. This is necessary to know for the characterization of our experiments, and is an important aspect of kinesin release and stepping behavior. We aim to answer this by comparing microtubule

release toward both directions in the absence of nucleotides when pulled from the head region with a free linker.

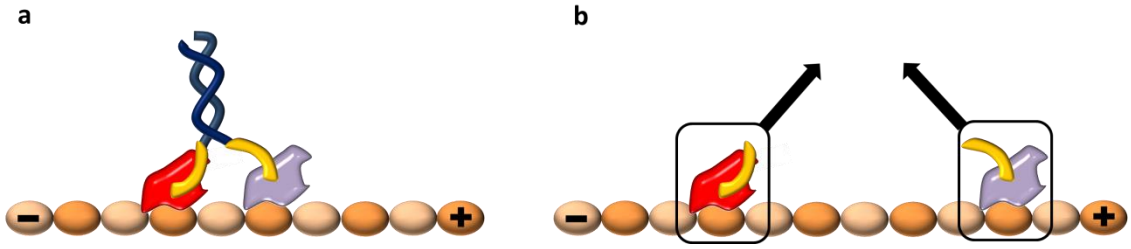

Figure 1.14. Front and rear heads of kinesin.
a) When kinesin is bound to the microtubule, front and rear heads of kinesin are in two different states.
b) We will represent these two states by pulling monomers forward or rearward.

1.7. References

[1] B. Alberts, A. Johnson, J. Lewis, M. Raff, K. Roberts, and P. Walker, *Molecular biology of the cell*. New York: Garland Science, 2008.

[2] A. D. Mehta, R. S. Rock, M. Rief, J. A. Spudich, M. S. Mooseker, and R. E. Cheney, "Myosin-V is a processive actin-based motor," *Nature*, vol. 400, no. 6744, pp. 590–593, Aug. 1999.

[3] R. S. Rock, S. E. Rice, A. L. Wells, T. J. Purcell, J. A. Spudich, and H. L. Sweeney, "Myosin VI is a processive motor with a large step size," *Proc. Natl. Acad. Sci.*, vol. 98, no. 24, pp. 13655–13659, Nov. 2001.

[4] A. P. Carter, "Crystal clear insights into how the dynein motor moves," *J. Cell Sci.*, vol. 126, no. 3, pp. 705–713, Feb. 2013.

[5] R. J. Stewart, J. P. Thaler, and L. S. Goldstein, "Direction of microtubule movement is an intrinsic property of the motor domains of kinesin heavy chain and Drosophila ncd protein," *Proc. Natl. Acad. Sci.*, vol. 90, no. 11, pp. 5209–5213, Jun. 1993.

[6] K. J. Verhey and J. W. Hammond, "Traffic control: regulation of kinesin motors," *Nat. Rev. Mol. Cell Biol.*, vol. 10, no. 11, pp. 765–777, Nov. 2009.

[7] G. M. Jeppesen and J. K. H. Hoerber, "The mechanical properties of kinesin-1: a holistic approach," *Biochem. Soc. Trans.*, vol. 40, no. 2, pp. 438–443, Apr. 2012.

[8] F. Jon Kull, E. P. Sablin, R. Lau, R. J. Fletterick, and R. D. Vale, "Crystal structure of the kinesin motor domain reveals a structural similarity to myosin," *Nature*, vol. 380, no. 6574, pp. 550–555, Apr. 1996.

[9] F. J. Kull, "Chapter 6 - Motor proteins of the kinesin superfamily: structure and mechanism," 01-May-2000. [Online]. Available: http://essays.biochemistry.org/bsessays/035/bse0350061.htm. [Accessed: 01-Jul-2013].

[10] F. Kozielski, S. Sack, A. Marx, M. Thormählen, E. Schönbrunn, V. Biou, A. Thompson, E.-M. Mandelkow, and E. Mandelkow, "The Crystal Structure of Dimeric Kinesin and Implications for Microtubule-Dependent Motility," *Cell*, vol. 91, no. 7, pp. 985–994, Dec. 1997.

[11] S. Rice, A. W. Lin, D. Safer, C. L. Hart, N. Naber, B. O. Carragher, S. M. Cain, E. Pechatnikova, E. M. Wilson-Kubalek, M. Whittaker, E. Pate, R. Cooke, E. W. Taylor, R. A. Milligan, and R. D. Vale, "A structural change in the kinesin motor protein that drives motility," *Nature*, vol. 402, no. 6763, pp. 778–784, Dec. 1999.

[12] A. Marx, A. Hoenger, and E. Mandelkow, "Structures of kinesin motor proteins," *Cell Motil. Cytoskeleton*, vol. 66, no. 11, pp. 958–966, 2009.

[13] S. S. Rosenfeld, P. M. Fordyce, G. M. Jefferson, P. H. King, and S. M. Block, "Stepping and Stretching HOW KINESIN USES INTERNAL STRAIN TO WALK PROCESSIVELY," *J. Biol. Chem.*, vol. 278, no. 20, pp. 18550–18556, May 2003.

[14] S. M. Block, C. L. Asbury, J. W. Shaevitz, and M. J. Lang, "Probing the kinesin reaction cycle with a 2D optical force clamp," *Proc. Natl. Acad. Sci.*, vol. 100, no. 5, pp. 2351–2356, Mar. 2003.

[15] J. M. Scholey, J. Heuser, J. T. Yang, and L. S. B. Goldstein, "Identification of globular mechanochemical heads of kinesin," *Nature*, vol. 338, no. 6213, pp. 355–357, Mar. 1989.

[16] L. A. Amos, “Kinesin from pig brain studied by electron microscopy,” *J. Cell Sci.*, vol. 87, no. 1, pp. 105–111, Feb. 1987.
[17] D. D. Hackney, J. D. Levitt, and J. Suhan, “Kinesin undergoes a 9 S to 6 S conformational transition.,” *J. Biol. Chem.*, vol. 267, no. 12, pp. 8696–8701, Apr. 1992.
[18] R. Cross and J. Scholey, “Kinesin: the tail unfolds,” *Nat. Cell Biol.*, vol. 1, no. 5, pp. E119–E121, Sep. 1999.
[19] G. Woehlke and M. Schliwa, “Walking on two heads: the many talents of kinesin,” *Nat. Rev. Mol. Cell Biol.*, vol. 1, no. 1, pp. 50–58, Oct. 2000.
[20] B. Gutiérrez-Medina, A. N. Fehr, and S. M. Block, “Direct measurements of kinesin torsional properties reveal flexible domains and occasional stalk reversals during stepping,” *Proc. Natl. Acad. Sci.*, vol. 106, no. 40, pp. 17007–17012, Oct. 2009.
[21] A. H. Crevenna, S. Madathil, D. N. Cohen, M. Wagenbach, K. Fahmy, and J. Howard, “Secondary Structure and Compliance of a Predicted Flexible Domain in Kinesin-1 Necessary for Cooperation of Motors,” *Biophys. J.*, vol. 95, no. 11, pp. 5216–5227, Dec. 2008.
[22] P. Bieling, I. A. Telley, J. Piehler, and T. Surrey, “Processive kinesins require loose mechanical coupling for efficient collective motility,” *EMBO Rep.*, vol. 9, no. 11, pp. 1121–1127, Nov. 2008.
[23] D. S. Friedman and R. D. Vale, “Single-molecule analysis of kinesin motility reveals regulation by the cargo-binding tail domain,” *Nat. Cell Biol.*, vol. 1, no. 5, pp. 293–297, Sep. 1999.
[24] J. Howard, A. J. Hudspeth, and R. D. Vale, “Movement of microtubules by single kinesin molecules,” *Nature*, vol. 342, no. 6246, pp. 154–158, Nov. 1989.
[25] S. M. Block, L. S. B. Goldstein, and B. J. Schnapp, “Bead movement by single kinesin molecules studied with optical tweezers,” *Nature*, vol. 348, no. 6299, pp. 348–352, Nov. 1990.
[26] D. D. Hackney, “Highly processive microtubule-stimulated ATP hydrolysis by dimeric kinesin head domains,” *Nature*, vol. 377, no. 6548, pp. 448–450, Oct. 1995.
[27] S. A. Endow and D. S. Barker, “Processive and Nonprocessive Models of Kinesin Movement,” *Annu. Rev. Physiol.*, vol. 65, no. 1, pp. 161–175, 2003.
[28] W. O. Hancock and J. Howard, “Processivity of the Motor Protein Kinesin Requires Two Heads,” *J. Cell Biol.*, vol. 140, no. 6, pp. 1395–1405, Mar. 1998.
[29] E. C. Young, H. K. Mahtani, and J. Gelles, “One-Headed Kinesin Derivatives Move by a Nonprocessive, Low-Duty Ratio Mechanism Unlike That of Two-Headed Kinesin†,” *Biochemistry (Mosc.)*, vol. 37, no. 10, pp. 3467–3479, Mar. 1998.
[30] E. Berliner, E. C. Young, K. Anderson, H. K. Mahtani, and J. Gelles, “Failure of a single-headed kinesin to track parallel to microtubule protofilaments,” *Nature*, vol. 373, no. 6516, pp. 718–721, Feb. 1995.
[31] A. Yildiz, M. Tomishige, R. D. Vale, and P. R. Selvin, “Kinesin Walks Hand-Over-Hand,” *Science*, vol. 303, no. 5658, pp. 676–678, Jan. 2004.
[32] S. S. Rosenfeld, J. Xing, G. M. Jefferson, H. C. Cheung, and P. H. King, “Measuring Kinesin’s First Step,” *J. Biol. Chem.*, vol. 277, no. 39, pp. 36731–36739, Sep. 2002.
[33] R. D. Vale and R. A. Milligan, “The Way Things Move: Looking Under the Hood of Molecular Motor Proteins,” *Science*, vol. 288, no. 5463, pp. 88–95, Apr. 2000.

[34] A. Yildiz, M. Tomishige, A. Gennerich, and R. D. Vale, “Intramolecular Strain Coordinates Kinesin Stepping Behavior along Microtubules,” *Cell*, vol. 134, no. 6, pp. 1030–1041, Sep. 2008.
[35] L. M. Klumpp, A. Hoenger, and S. P. Gilbert, “Kinesin’s second step,” *Proc. Natl. Acad. Sci. U. S. A.*, vol. 101, no. 10, pp. 3444–3449, Mar. 2004.
[36] D. D. Hackney, “Kinesin ATPase: rate-limiting ADP release,” *Proc. Natl. Acad. Sci.*, vol. 85, no. 17, pp. 6314–6318, Sep. 1988.
[37] Y.-Z. Ma and E. W. Taylor, “Interacting Head Mechanism of Microtubule-Kinesin ATPase,” *J. Biol. Chem.*, vol. 272, no. 2, pp. 724–730, Jan. 1997.
[38] S. P. Gilbert, M. L. Moyer, and K. A. Johnson, “Alternating Site Mechanism of the Kinesin ATPase†,” *Biochemistry (Mosc.)*, vol. 37, no. 3, pp. 792–799, Jan. 1998.
[39] H. S. Sardar and S. P. Gilbert, “Microtubule Capture by Mitotic Kinesin Centromere Protein E (CENP-E),” *J. Biol. Chem.*, vol. 287, no. 30, pp. 24894–24904, Jul. 2012.
[40] K. Svoboda, C. F. Schmidt, B. J. Schnapp, and S. M. Block, “Direct observation of kinesin stepping by optical trapping interferometry,” *Nature*, vol. 365, no. 6448, pp. 721–727, Oct. 1993.
[41] C. L. Asbury, A. N. Fehr, and S. M. Block, “Kinesin Moves by an Asymmetric Hand-Over-Hand Mechanism,” *Science*, vol. 302, no. 5653, pp. 2130–2134, Dec. 2003.
[42] D. D. Hackney, “Evidence for alternating head catalysis by kinesin during microtubule-stimulated ATP hydrolysis.,” *Proc. Natl. Acad. Sci. U. S. A.*, vol. 91, no. 15, pp. 6865–6869, Jul. 1994.
[43] A. Hoenger, S. Sack, M. Thormahlen, A. Marx, J. Muller, H. Gross, and E. Mandelkow, “Image Reconstructions of Microtubules Decorated with Monomeric and Dimeric Kinesins: Comparison with X-Ray Structure and Implications for Motility,” *J. Cell Biol.*, vol. 141, no. 2, pp. 419–430, Apr. 1998.
[44] W. O. Hancock and J. Howard, “Kinesin’s processivity results from mechanical and chemical coordination between the ATP hydrolysis cycles of the two motor domains,” *Proc. Natl. Acad. Sci.*, vol. 96, no. 23, pp. 13147–13152, Nov. 1999.
[45] K. Kaseda, H. Higuchi, and K. Hirose, “Alternate fast and slow stepping of a heterodimeric kinesin molecule,” *Nat. Cell Biol.*, vol. 5, no. 12, pp. 1079–1082, Dec. 2003.
[46] K. C. Rank and I. Rayment, “Functional asymmetry in kinesin and dynein dimers,” *Biol. Cell*, vol. 105, no. 1, pp. 1–13, 2013.
[47] A. Hoenger, M. Thormählen, R. Diaz-Avalos, M. Doerhoefer, K. N. Goldie, J. Müller, and E. Mandelkow, “A new look at the microtubule binding patterns of dimeric kinesins,” *J. Mol. Biol.*, vol. 297, no. 5, pp. 1087–1103, Apr. 2000.
[48] A. Yildiz and P. R. Selvin, “Kinesin: walking, crawling or sliding along?,” *Trends Cell Biol.*, vol. 15, no. 2, pp. 112–120, Feb. 2005.
[49] N. J. Carter and R. A. Cross, “Mechanics of the kinesin step,” *Nature*, vol. 435, no. 7040, pp. 308–312, May 2005.
[50] J. E. Molloy and S. Schmitz, “Molecular motors: Kinesin steps back,” *Nature*, vol. 435, no. 7040, pp. 285–287, May 2005.
[51] N. J. Carter and R. A. Cross, “Kinesin’s moonwalk,” *Curr. Opin. Cell Biol.*, vol. 18, no. 1, pp. 61–67, Feb. 2006.

[52] S. M. Block, “Kinesin Motor Mechanics: Binding, Stepping, Tracking, Gating, and Limping,” *Biophys. J.*, vol. 92, no. 9, pp. 2986–2995, May 2007.
[53] A. Gennerich and R. D. Vale, “Walking the walk: how kinesin and dynein coordinate their steps,” *Curr. Opin. Cell Biol.*, vol. 21, no. 1, pp. 59–67, Feb. 2009.
[54] M. C. Alonso, D. R. Drummond, S. Kain, J. Hoeng, L. Amos, and R. A. Cross, “An ATP Gate Controls Tubulin Binding by the Tethered Head of Kinesin-1,” *Science*, vol. 316, no. 5821, pp. 120–123, Apr. 2007.
[55] S. Uemura, K. Kawaguchi, J. Yajima, M. Edamatsu, Y. Y. Toyoshima, and S. Ishiwata, “Kinesin–microtubule binding depends on both nucleotide state and loading direction,” *Proc. Natl. Acad. Sci.*, vol. 99, no. 9, pp. 5977–5981, Apr. 2002.
[56] S. Uemura and S. Ishiwata, “Loading direction regulates the affinity of ADP for kinesin,” *Nat. Struct. Mol. Biol.*, vol. 10, no. 4, pp. 308–311, Apr. 2003.
[57] N. R. Guydosh and S. M. Block, “Backsteps induced by nucleotide analogs suggest the front head of kinesin is gated by strain,” *Proc. Natl. Acad. Sci.*, vol. 103, no. 21, pp. 8054–8059, May 2006.
[58] B. E. Clancy, W. M. Behnke-Parks, J. O. L. Andreasson, S. S. Rosenfeld, and S. M. Block, “A universal pathway for kinesin stepping,” *Nat. Struct. Mol. Biol.*, vol. 18, no. 9, pp. 1020–1027, Sep. 2011.
[59] E. Toprak, A. Yildiz, M. T. Hoffman, S. S. Rosenfeld, and P. R. Selvin, “Why kinesin is so processive,” *Proc. Natl. Acad. Sci.*, vol. 106, no. 31, pp. 12717–12722, Aug. 2009.
[60] N. R. Guydosh and S. M. Block, “Direct observation of the binding state of the kinesin head to the microtubule,” *Nature*, vol. 461, no. 7260, pp. 125–128, Sep. 2009.
[61] A. Krebs, K. N. Goldie, and A. Hoenger, “Complex Formation with Kinesin Motor Domains Affects the Structure of Microtubules,” *J. Mol. Biol.*, vol. 335, no. 1, pp. 139–153, Jan. 2004.
[62] M. Kikkawa, “The role of microtubules in processive kinesin movement,” *Trends Cell Biol.*, vol. 18, no. 3, pp. 128–135, Mar. 2008.
[63] C. V. Sindelar and K. H. Downing, “An atomic-level mechanism for activation of the kinesin molecular motors,” *Proc. Natl. Acad. Sci.*, vol. 107, no. 9, pp. 4111–4116, Mar. 2010.
[64] C. V. Sindelar, “A seesaw model for intermolecular gating in the kinesin motor protein,” *Biophys. Rev.*, vol. 3, no. 2, pp. 85–100, Jun. 2011.

Chapter 2. Methods

2.1. Introduction to optical trapping

Optical trapping was first introduced by Arthur Ashkin when he showed that radiation pressure from a laser can accelerate and trap micron-sized particles [1,2] and built the first three-dimensional optical trap [3]. An optical trap provides the ability to apply picoNewton level forces to small objects down to a few nanometers in size, while measuring displacement in nanometers [4]. This capability makes it an ideal tool for studying physical and biological systems. Particularly in single molecule studies of molecular motors, optical traps have been crucial, as evident in wide-spread applications [5–22]. Most common geometries for optical trapping involve a micron sized bead that is attached to a biological specimen, and the specimen is investigated by optically manipulating the bead position and applying a force on the bead that is propagated to the specimen (Figure 2.1).

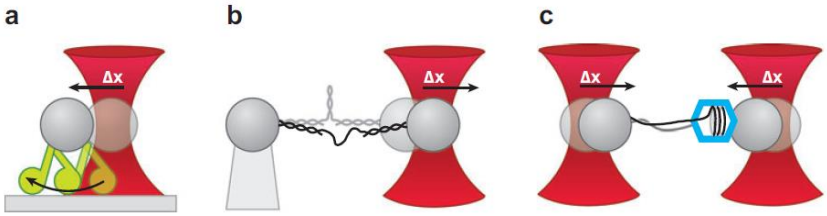

Figure 2.1. Different geometries for optical trapping.
a) A molecular motor is attached to a bead that is optically trapped, and is walking on a filament attached to the glass surface [12,23,24]. **b)** To observe unfolding, an RNA hairpin is attached to two different beads at its two ends. One of the beads is optically manipulated while the other one is held stationary [25–28]. **c)** A DNA packed with a bacteriophage portal motor is tethered to two beads both of which are trapped separately. Relative motions of the beads are measured [29,30]. (Figure from [31])

2.1.1. How optical traps work

To trap a small dielectric object, a small force is exerted on it by tightly focusing a laser beam with a high numerical aperture objective. This results in two forces acting on the object. The first one is the scattering force in the direction of beam propagation that arises when photons hit the object and scatter. The second force is due to the strong electric field gradient near the beam waist, and the object experiences a force in the direction of this gradient [4,32]. Because three-dimensional trapping requires a very steep gradient, the gradient force component is large, and the equilibrium position of the object is slightly shifted from the focal point [4]. For small displacements of the object from the trap center, the force is linearly proportional to displacement, and the system can be thought of as a spring obeying Hooke's law (Figure 2.2).

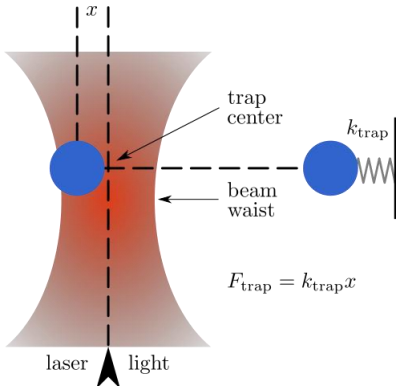

Figure 2.2. Position of the trapped bead.
The trapped bead is slight above the focal point. Displacements from its center can be approximated by Hooke's law. (Figure from [33])

For theoretical analysis, two limiting cases can be easily examined, i.e. when the dielectric object is much smaller or much larger than the wavelength of the laser. The calculations for intermediate cases are non-trivial.

2.1.2. The ray optics regime

The relevant case for our study is when the trapped bead is much larger than the wavelength of the laser (d>>λ), and is shifted sideways from the laser focus. In this case, the optical forces can be readily calculated with simple ray optics [4,34]. Figure 2.3a shows a force diagram with two rays. In the absence of the bead, the rays coming through the objective are directed towards the true laser focus *f*. The bead that is positioned to the right of the beam deflects the rays and the new focus is shifted to the right. An equal and opposite momentum change of the rays is imparted to the bead. The resulting force on the bead is directed towards left and is linearly proportional to the light intensity.

It is more realistic to consider a Gaussian beam shape as in Figure 2.3b, where rays closer to the beam center have a higher intensity than rays closer to the edge. Here too, the net force on the beam points towards left.

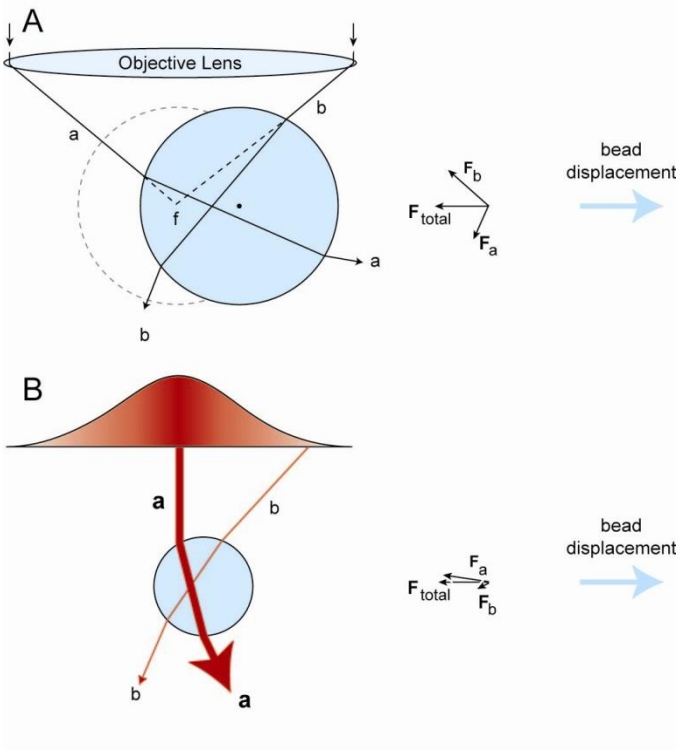

Figure 2.3. Forces in the ray optics regime.
a) Simple ray diagram with two rays, a and b. Due to refraction through the bead, the focus is shifted to the right. Momentum from both rays results in an equal and opposite momentum change on the bead, and the net force on the bead resulting from forces F_a and F_b is directed to the left. **b)** A Gaussian intensity profile for the beam is shown, where rays closer to center have higher intensity. The net force on the bead caused by rays in this profile also points to the left for a bead that is initially positioned towards the right. (Figure from [34])

2.2. Optical Trap Design and Elements

2.2.1. Optical Trap Setup and Components

A commercial Nikon Ti-Eclipse microscope has been used to build the optical trap. This microscope provides the bright field illumination and imaging ports. There are four lasers in the setup. The trapping laser is 1064 nm and forms the trap in the image plane. An 845 nm focusing laser is used to track the height of the coverslip and achieve stability in the z-axis by performing active feedback on the z-position of the sample. There are two different lasers that can be used for TIRF, namely a 488 nm blue laser and a 633 nm red laser. The layout of the optical trap is shown in Figure 2.4.

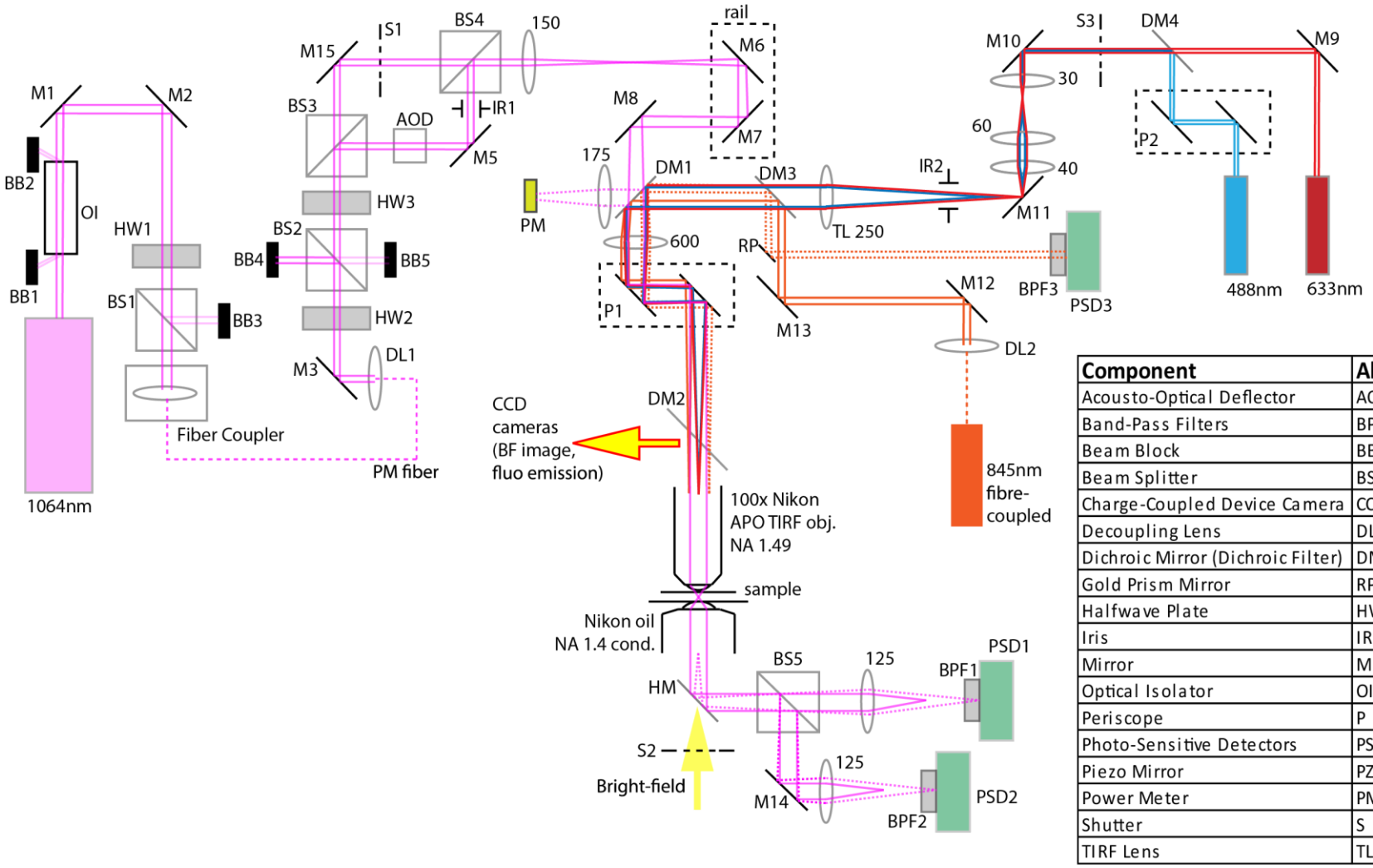

Component	Abbr.
Acousto-Optical Deflector	AOD
Band-Pass Filters	BPF
Beam Block	BB
Beam Splitter	BS
Charge-Coupled Device Camera	CCD
Decoupling Lens	DL
Dichroic Mirror (Dichroic Filter)	DM
Gold Prism Mirror	RP
Halfwave Plate	HW
Iris	IR
Mirror	M
Optical Isolator	OI
Periscope	P
Photo-Sensitive Detectors	PSD
Piezo Mirror	PZM
Power Meter	PM
Shutter	S
TIRF Lens	TL

Figure 2.4. Layout of Yildiz Lab optical trap.
The schematic shows the optical elements and their arrangement in the optical trap. Four different laser pathways are shown in pink (1064 nm), blue (488 nm), red (633 nm) and orange (845 nm). Lenses are denoted by their focal length, e.g. 125 for a lens with 125 mm focal length. (Figure c/o Vladislav Belyy)

2.2.2. Laser

A good trapping laser delivers a Gaussian mode output that focuses to the smallest diameter beam waist, and is expected to have low power fluctuations and high pointing stability [4]. Our trapping laser is a 2W CW 1064nm (NIR-Class 4) neodymium:yttrium–orthovanadate sNd:YVO4d laser (Compass 1064, Coherent Inc.), which provides nominally collimated and linearly polarized Gaussian beam. The wavelength of the laser is within the preferred range for working with biological specimens (750-1200nm) where the damage caused by absorption of the laser by the specimen is reduced greatly compared to the visible range [35].

An optical isolator (OI) was used to prevent back-reflected beams from reentering the laser head and causing instabilities. Upon leaving the optical isolator, these back-reflections are blocked with beam blocks (BB1 and BB2). In order to improve pointing stability of the laser and minimize unwanted movements of the trap position, the laser has been fiber-coupled into a polarization maintaining fiber. To guarantee that the beam enters the fiber with only the desired polarization, a beam splitter (BS1) is used to clean it off of all the other polarizations. At the exit end of the fiber, the laser is decoupled with a pigtailed collimating lens (DL1) which produces a 2.4 mm diameter Gaussian beam.

Laser power can be adjusted by polarization. By rotating a halfwave plate (HW2), only a certain amount of the beam is passed through the beam splitter (BS2) and the rest if caught by a high-power beam block (BB4). In our setup, the laser is split into two different paths by a beam splitter (BS3), and the relative powers in these paths are controlled by the addition of another halfwave plate (HW3).

The laser beam in our setup is split into two orthogonally polarized paths, allowing us to simultaneously create two independent traps in the image plane. One of the beams goes through the acousto-optic deflector (AOD) while the other one is steered by a piezo mirror. These two paths are recombined before entering the objective.

2.2.3. Objective

The efficiency of the optical trap depends critically on the objective, which determines the stiffness of the trap in response to laser power [4]. Our objective is a 100x oil immersion 1.49 NA Plan-Apo Nikon objective. Ideally, the beam width should slightly overfill the back aperture of the objective to maximize the trapping force while minimizing power loss caused by the clipping of the beam by the objective. This is achieved in our setup by forming a 4x Keplerian telescope with 150 mm and 600 mm lenses. Two of the mirrors (M6 and M7) between these lenses are mounted on a rail to adjust the path length and move the trap position in the z-direction relative to the image plane.

In our microscope, the Z-height is controlled by a true piezo stage and the X/Y stage is moved by piezo-driven servos.

2.2.4. Beam Steering and Dynamic Position Control

To move the bead to a desired position in the field-of-view, different strategies were used to dynamically control the trap position. The power of the laser beam also needs to be adjusted by a custom software to adjust the trap stiffness [4]. In our setup, the trap position is adjusted by the acousto-optic deflector (AOD), while the trap stiffness is controlled by the halfwave plate and BS cube upstream from the AOD.

An AOD contains a crystal bound to a piezo-electric transducer on one side and an acoustic absorber on the other side. Ultrasound waves travelling across the crystal form an optical diffraction gating, the period of which depends on the wavelength of the acoustic waves. A laser beam incident at Bragg angle θ gets diffracted in the crystal as illustrated in Figure 2.5. The first order diffracted light gets deflected by an angle ϕ that depends on the frequency of the sound wave as $\Delta\phi = (\lambda / \upsilon)\Delta f$ where λ is the wavelength, v is the velocity of the sound wave, and f is the acoustic frequency. Trap position can be varied by changing the acoustic frequency and thereby deflecting the beam to different positions. Trap stiffness can be also controlled with an AOD by changing the amplitude of the sound wave and hence the intensity of the laser light [4,36].

It is important that the AOD is in a plane conjugate to the back-focal plane (BFP) of the objective to move the trap in an image plane without changing its angle.

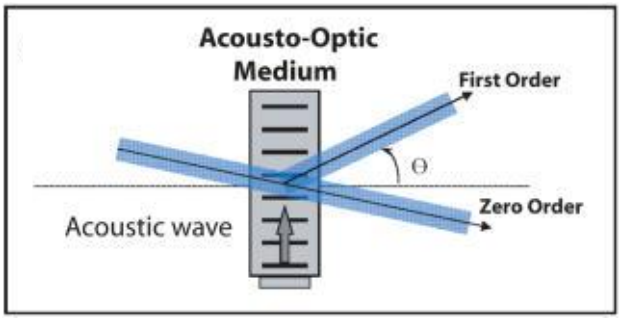

Figure 2.5. Working principle of an acousto-optic deflector
A laser beam entering the AOD gets diffracted by the sound waves inside the crystal and gets deflected upon exiting the crystal by an angle . The gating period of the sound waves can be varied, which allows for deflecting the laser beam to a desired position. AOD response is really fast, such that it doesn't limit the time response of an optical trap. (Figure from [37])

2.2.5. Position Detection

Measuring nanoscale forces and distances means the optical trap system must have very sensitive position detection capabilities and precise calibration methods. For precision, it is imperative to use spherical beads because this greatly simplifies the calibration process, and all the position detection and calibration methods are based on the assumption that the beads are spherical [4].

In our system, a second dichoric mirror is mounted on the condenser side to uncouple the laser light from the illuminating light. Position detection is done with back focal plane (BFP) interferometry using the same 1064 nm trapping laser. With this method, the centroid of the interference pattern between the scattered and unscattered rays in the BFP is determined. A beam splitter (BS5) separates the piezo and AOD paths. The BFP of the condenser is imaged onto a photosensitive detector (PSD). To do this correctly, the position where the PSD is mounted needs to be calculated exactly. Bandpass filters (BPF) and neutral density (ND) filters ensure that only 1064 nm light is incident on the PSD and the signal from the PSD is not saturated above the threshold.

2.2.6. Calibration

2.2.6.1. Force Calibration and Stiffness Determination

Force calculation in an optical trap relies on Hooke's law, $F = -kx$, where *F* is the force, *k* is the trap stiffness and *x* is the bead displacement. It is therefore an indirect measurement based on measuring displacement and determining the trap stiffness [4]. In our experiments, the trap stiffness is calibrated anew for each sample. We use beads of uniform radius, and fit the power spectrum of a trapped bead into a one-sided Lorentzian curve which describes the thermal fluctuations of a trapped object [4].

One way to write the Lorentizan equation is:

$$S(f) = \frac{S_0 f_0^2}{f_0^2 + f^2}$$

where S_0 is the asymptotic power, f_0 the corner frequency and *f* the frequency [36]. The corner frequency is directly correlated to the trap stiffness as

$$f_0 = \frac{k}{2\pi\gamma}$$

$$\gamma = 6\pi\eta r$$

where the drag coefficient γ is given by Stokes Law for a drag over a sphere, where η is the viscosity of the medium and r is the radius of the sphere. To avoid any surface effects on the drag, we calibrate trap stiffness 3 μm into the solution, where the Stokes drag approximation becomes very accurate.

2.2.6.2. Position Calibration

In order to accurately determine the bead displacement (and applied force which is based on it), position calibration must be as precise as possible. To achieve such precision, we perform stepwise calibration. First the CCD pixel size is calibrated using the reticle lines (100 nm per line). Second, AOD driving frequency and the trap position in the image plane are calibrated by using a stuck bead and imaging it at different positions along both axes to infer the relationship. Lastly, a free bead is trapped and brought to a height equivalent to experiments. It is then scanned in both x- and y-axes and the position signals are recorded to determine the calibration coefficients. Figure 2.6 shows the cubic fit for the PSD response. The linear range of our PSD is within 150 nm from the trap center, but we use the full cubic fit in our calculations instead of the linear approximation.

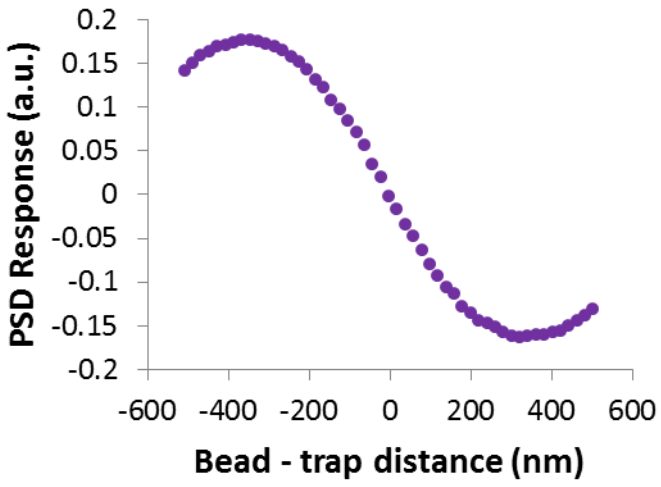

Figure 2.6. PSD response curve
Linear range of the PSD is within approximately 150 nm from the trap center.

2.2.7. Total Internal Reflectance Fluorescence Microscopy

Having the ability to observe single molecules with fluorescence, while simultaneously trapping and manipulating the biological specimens offers a big advantage in single molecule studies. Our setup incorporates this ability with the addition of two total internal reflectance

fluorescence (TIRF) lines. TIRF microscopy is based on light getting totally internally reflected at the coverslip liquid interface and only an evanescent wave penetrating into the flow channel that illuminates a region about a 100 nm above the coverslip (Figure 2.7). Since the elements in the background are eliminated, the signal to noise ration near the surface is very high and enables single molecules to be discriminated.

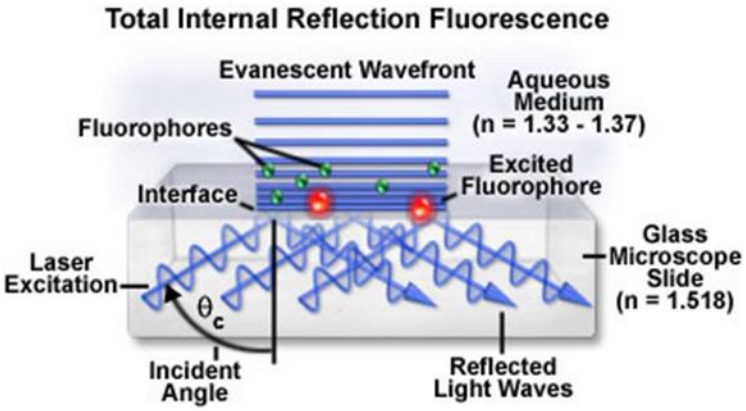

Figure 2.7. Total Internal Reflectance Fluorescence
The laser light is totally reflected at the coverslip/liquid interface. Only the fluorophores closest to the surface are excited and hence the background fluorescence is greatly diminished to allow single molecules to be differentiated. (Figure from [38])

The TIRF lines in our setup consist of a blue 488 nm and a red 633 nm laser and are used to detect fluorescently labeled axonemes and dyneins that accumulate on the (-) of the axonemes.

2.2.8. Noise elimination

In order to eliminate noise due to environmental factors, several precautions have been implemented. The microscope has been built in a temperature controlled room (±0.1˚ C) to minimize thermal fluctuations. The room is acoustically sealed and power supplies, control boxes and the computer are moved outside the microscope room to minimize acoustic noise and thermal instability. To prevent air currents from affecting the experiments, the microscope room has its own ventilation system separate from the building and temperature and speed of the ventilated air is controlled to reduce temperature gradient and air flow within the room. In addition, the microscope is enclosed to further isolate the setup from the environment. The entire setup is built on an air table that diminishes mechanical vibrations. Microscope optics are rigidly mounted to the table by using ultra-stable stainless steel mounts purchased from Newport Inc. All experiments are done when once the system power has stabilized and temperature inside the enclosure reaches the equilibrium.

2.2.9. Computer Control of Optical Trap

The optical trap is controlled remotely from an adjacent control room via a computer that runs custom software written in LabVIEW. There are three main components of the control hardware, which are the main computer, a field-programmable gate array (FPGA) and a network connected NI CompactRIO system. The computer connects to the CompactRIO system, and the CompactRIO connects to the FPGA. The user has control of the system via Host PC, which sends network variables to the CompactRIO and FPGA chip and receives data in real time through a proprietary NI protocol called Network Stream. The FPGA chip and Trap PC deal directly with hardware.

2.3. Biochemical Methods

2.3.1. Preparation of kinesin constructs

Plasmids for human kinesin-1 monomers, which contain first 349 amino acids from the N-terminus (K349) was generously provided by Ronald Vale from UCSF. The construct has the entire motor domain including the neck linker and a region of the neck coiled coil. In order to label kinesin specifically with biotin maleimide, we used cysteine light kinesin with all surface exposed cysteines were changed to alanine [39]. We next introduced E215C mutation (Figure 2.8a) for maleimide labeling [40]. We use this construct to apply load on the monomer by pulling from the head region.

The plasmid we received for the second construct, K339-GFP, is a modified version of the first one with a green fluorescent protein (GFP) inserted at the C-terminus of the neck-linker is shown in Figure 2.8b, and the last 10 amino acids removed. We have inserted the missing 10 amino acids to obtain K349-GFP, identical in length to K349-E215C, for reliable comparison of results obtained with these constructs. GFP was also replaced with HaloTag (Promega Inc.) for crosslinking a DNA tether to the C-terminal end of kinesin-1, using QuickChange® site directed mutagenesis methods (Strategene).

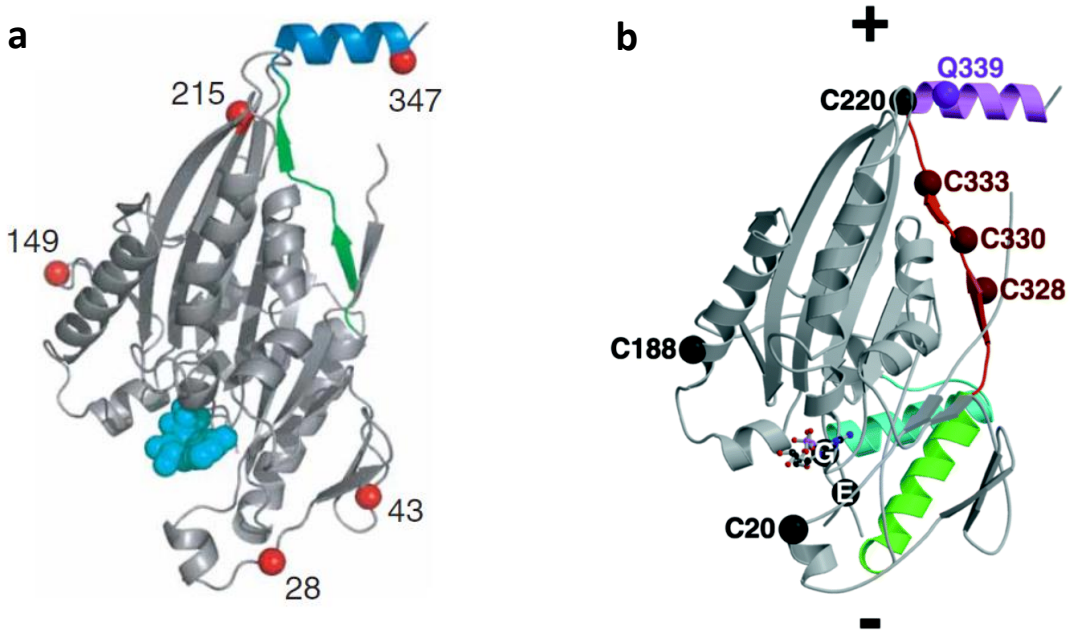

Figure 2.8. Structure of kinesin349 monomer
a) Structure of the K349-E215C kinesin monomer construct gifted by Ronald Vale. Red spheres show several sites where Cysteines can be introduced. Our construct has the Cysteine at the site labeled as 215. Neck linker is shown green, neck coiled coil is shown blue, and ADP space-fill is shown in cyan. (Figure from [40]) **b)** Same structure for kinesin349 in different colors, which shows the junction point for the kinesin339-GFP protein as the purple sphere labeled Q339. (Figure from [39])

2.3.1.1. Protein expression

Plasmids have been first transformed into *Escherichia coli*. Both plasmids have been mixed with 20 µl XL1 blue cells on ice for 30 minutes, followed by a heat shock at 42 ^{o}C for 45 seconds. After mixing with 400 µl S.O.C. media, the cells have been incubated on a shaker at 37 ^{o}C for an hour. Next, the cells have been plated on to Ampicillin resistant plates and incubated overnight at 37 ^{o}C. Following day, four colonies from each plate have been chosen and grown in LB-media with Ampicillin overnight on a shaker at 37 ^{o}C. To extract the plasmids, QIAprep Spin Miniprep kit has been used according to its protocol, which yielded 50 ul of each plasmid confirmed by sequencing results.

Transformation of these plasmids into Rosetta cells has been done similarly. Inoculation of large-scale cultures was done in 1 liter LB-Media with Ampicillin at 37 ^{o}C. Growth has been monitored by checking the O.D. and stopped before saturation. Once the solution has cooled down to room temperature, IPTG was added and growth continued at 19 ^{o}C on a shaker overnight.

Cells have been harvested by spinning down at 5000 rpm for 20 min at 4 ^{o}C. Resulting pellets have been suspended in lysis buffer (50 mM NaH_2PO_4, 250 mM NaCl, 2 mM $MgCl_2$, 20 mM Imidazole, pH 8) with the addition of 1 mM ATP, 10 mM βME and 1 mM PMSF. The solution has been sonicated twice by repeated pulse and pause for 2 minutes. Lastly, the solution has been spinned in an ultracentrifuge at 40000 rpm for 30 minutes at 4 ^{o}C. The supernatant that contains the proteins has been mixed with beads for purification in an Ni-NTA agarose affinity column. After flowing the protein/Ni-NTA agarose mixture through the column, the column has been washed with 10 ml of Ni wash buffer (50 mM NaH_2PO_4, 250 mM NaCl, 1 mM $MgCl_2$, 20 mM Imidazole, pH 6 with the addition of 0.1 mM ATP and 10 mM βME before use) five times and the protein has been eluted by applying 1 ml of Ni elution buffer (50 mM NaH_2PO_4, 250 mM NaCl, 1 mM $MgCl_2$, 500 mM Imidazole, pH 7.2 with the addition of 0.1 mM ATP and 10 mM βME before use) and collecting the flow-through for a total of five times.

Protein expression has been confirmed with a protein gel as shown in Figure 2.9, and concentrations have been measured in NanoDrop. For K349-E215C, using absorption at 280 nm with an extinction coefficient of 22920 M^{-1} cm^{-1} has been used, concentration was found to be around 177 µM. For K339-GFP, concentration has been measured using GFP absorption at 488 nm, calculated with GFP extinction coefficient of 55000 M^{-1} cm^{-1}, and found to be around 43 µM.

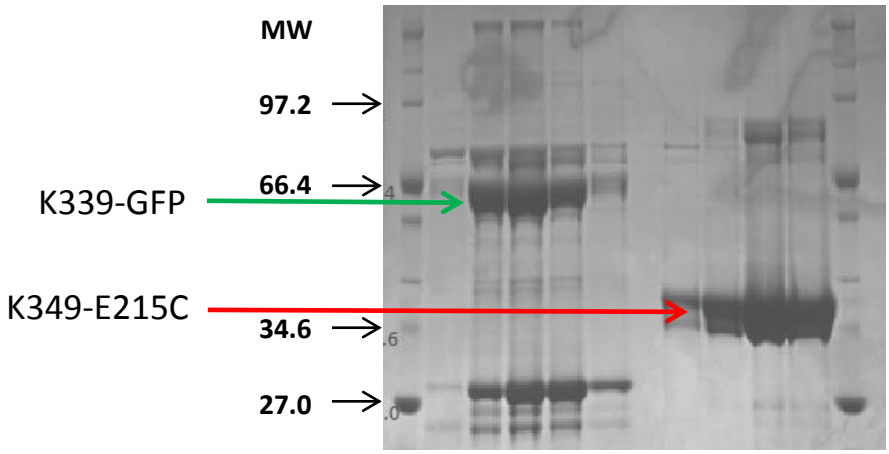

Figure 2.9. Results for protein expression of K349-E215C and K339-GFP
Protein expression has been confirmed with a denaturing PAGE gel. Lanes 1-5 are K339-GFP with a molecular weight of 65 kDa. Lanes 7-10 are K349-E215C with a molecular weight of 40 kDa.

2.3.1.2. Purification of K349-E215C

Prior to further preparation of the K349-E215C construct for the optical trap assay, we have purified the kinesin monomer with a microtubule bind and release (MTBR) protocol [41] that separates out the active motors from the inactive ones according to their ability to bind to the microtubules. Once mixed, active motors bind to microtubules and are spun down, while the

supernatant with inactive motors is discarded. Microtubules are then suspended in solution and the active motors are released by addition of ATP and 300 mM KCl, separated from the microtubules by spinning down the microtubules, and collecting the resulting motor solution. Figure 2.10 shows the gel results of MTBR purification with samples from every step that lead to it.

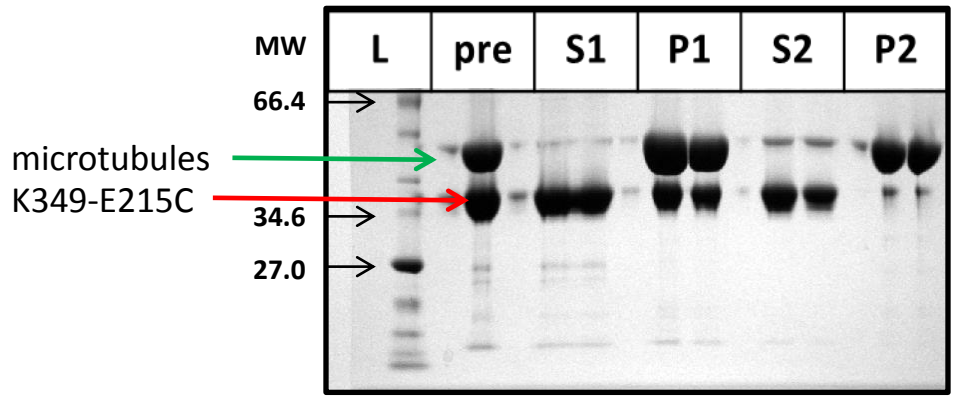

Figure 2.10. Purification of K349-E215C by MTBR
Lanes in the gels have been labeled to show **L)** Protein ladder **pre)** Microtubule (MT) and motor mixture **S1)** Supernatant with inactive motors **P1)** MT with active motors bound **S2)** Recovered active motors used in the rest of the study **P2)** MT after separation from motor

2.3.1.3. DNA-Labeling of K349-E215C

To attach kinesin monomers to beads for optical trapping, we have used a double stranded DNA as a crosslinker. Both strands have 74 base pairs and have been custom made by IDT. One of the strands has been modified with biotin on 5' side (/5Biosg/TTC GGT CAA TAC CCG GCG CAG AGC GCT CAG GCG CGA GGT CAA CAG AGG GCG GAG GGT GGG CCA GCG CGA CCC CG) and the other strand has been modified with a free amine also on the 5' side (/5AmMC6/GTG TCG GGG TCG CGC TGG CCC ACC CTC CGC CCT CTG TTG ACC TCG CGC CTG AGC GCT CTG CGC CGG GTA TTG AC). While the free amine on the DNA strand serves for kinesin conjugation, the biotin serves for attachment to streptavidin-coated beads (Figure 2.11).

The binding strategy to attach the double-stranded DNA to the K349-E215C construct involves conjugating the free amine on the DNA to the cysteine on the kinesin monomer via Sulfo-SMCC coupling. Sulfo-SMCC is an 8 Å crosslinking agent for amine to sulfhydryl binding. First, its NHS-ester is reacted with the free amine on the DNA and then the maleimide reactive group binds to the cysteine on the kinesin. Figure 2.11b shows the resulting compound, while Figure 2.11c shows the Sulfo-SMCC structure and the reactive groups it binds.

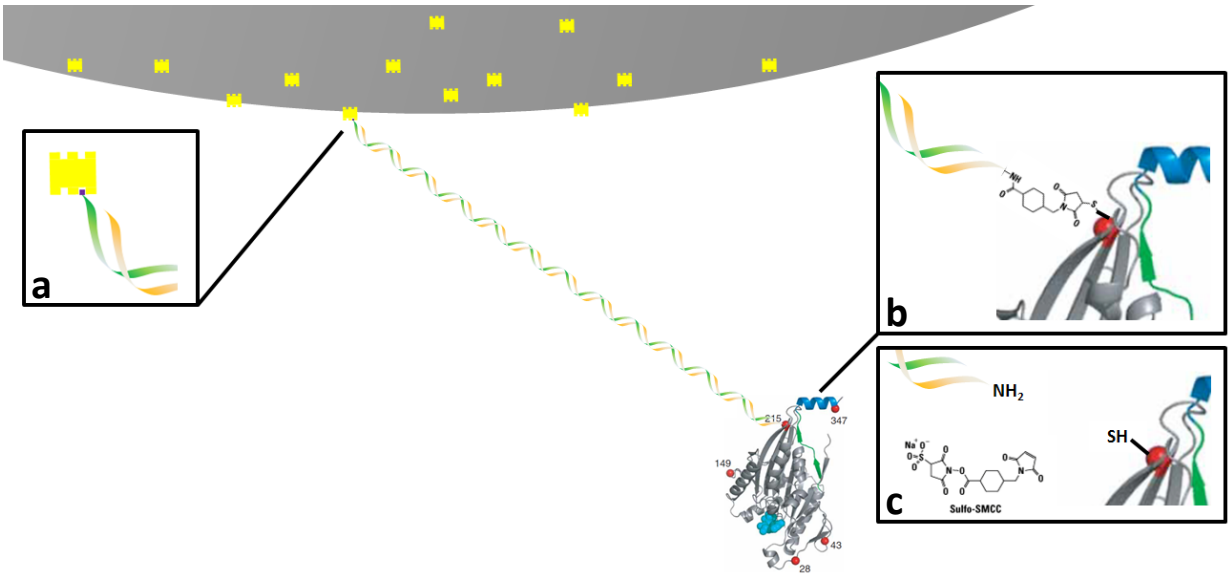

Figure 2.11. DNA-crosslinker for bead-motor attachment of K349-E215C
Streptavidin-coated beads are connected to the kinesin monomer via DNA crosslinker. **a)** DNA is attached to the beads via biotin (purple) streptavidin (yellow) interaction. **b)** DNA is conjugated to the free cysteine on the kinesin monomer with Sulfo-SMCC as crosslinker. **c)** The reactive groups in the DNA-kinesin coupling. Free amine on the DNA reacts with the NHS-ester of Sulfo-SMCC, sulfhydryl group on the cysteine reacts with the maleimide group of the Sulfo-SMCC.

For the reaction, first the DNA oligos have been hybridized by combining 30 µl each of 100 mM oligo solutions with 20 µl of DNA buffer (80 mM $NaHCO_3$ pH 8.4, 200 mM KCl, 5 mM $MgCl_2$), heating at 90 ^{o}C for 2 minutes and cooling to 25 ^{o}C for 40 minutes. Sulfo-SMCC (Pierce) has been prepared in 40x excess and 5 µl of it has been added to the DNA solution. After incubation for 90 minutes in 37 ^{o}C, excess Sulfo-SMCC has been removed by desalting through Illustra MicroSpin G-25 columns twice. Desalting reduced the DNA concentration to about half the initial concentration. All the resulting DNA-SMCC has been mixed with kinesin K349-E215 in 1:1 DNA to kinesin ratio, and reacted overnight at 4 ^{o}C. For control purposes, two parallel reactions have been tested, using less DNA concentration and using a Cy3 labeled DNA strand. To verify conjugation of DNA and kinesin, a protein gel was run. Two sets of each reaction were run in left and right halves of the gel, the gel has then been cut into two to stain in two different ways. The first half was coomassie-stained to detect the protein, and the second half was stained with methylene blue to detect the DNA. The results are shown in Figure 2.12. The kinesin-DNA conjugate appears in the same location in both cases, which verifies binding.

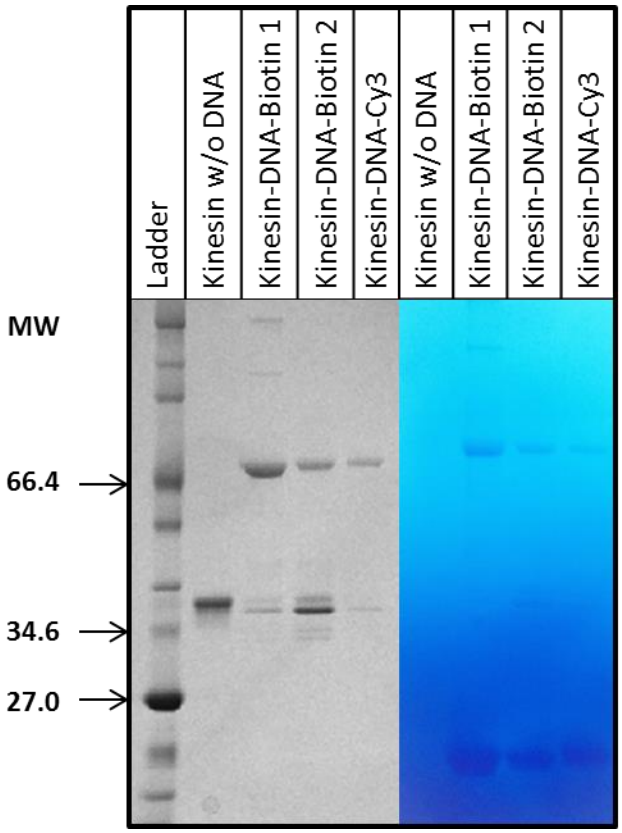

Figure 2.12. Kinesin-DNA labeling results for K349-E215C
Protein gel shows the results of labeling K349-E215C with DNA. **The first half of the gel** is stained with coomassie blue. The *first lane* is ladder, the *second lane* is kinesin without any DNA, *third lane* is the product from kinesin:DNA (1:1) reaction showing the protein at a higher molecular weight consistent with DNA attachment and only a trace amount of kinesin left unlabeled. *Fourth lane* is kinesin:DNA (3:1) reaction, with some free kinesin and some DNA-conjugated kinesin. *Fifth lane* is the kinesin:DNA-Cy3 reaction. **Second half of the gel** has the identical components. This half is stained with methylene blue that colors DNA but not the proteins. Lanes with Kinesin-DNA stain the DNA at the same location corresponding to protein staining and show excess DNA at the bottom of the gel. This confirms that DNA is indeed bound to kinesin monomers.

2.3.1.4. Protein expression and purification of K349-HT

A protein expression was done similarly as before and the results were verified with a protein gel seen in Figure 2.13a. For purification, another MTBR assay was carried out and the results of the procedure are seen in the gel shown in Figure 2.13b.

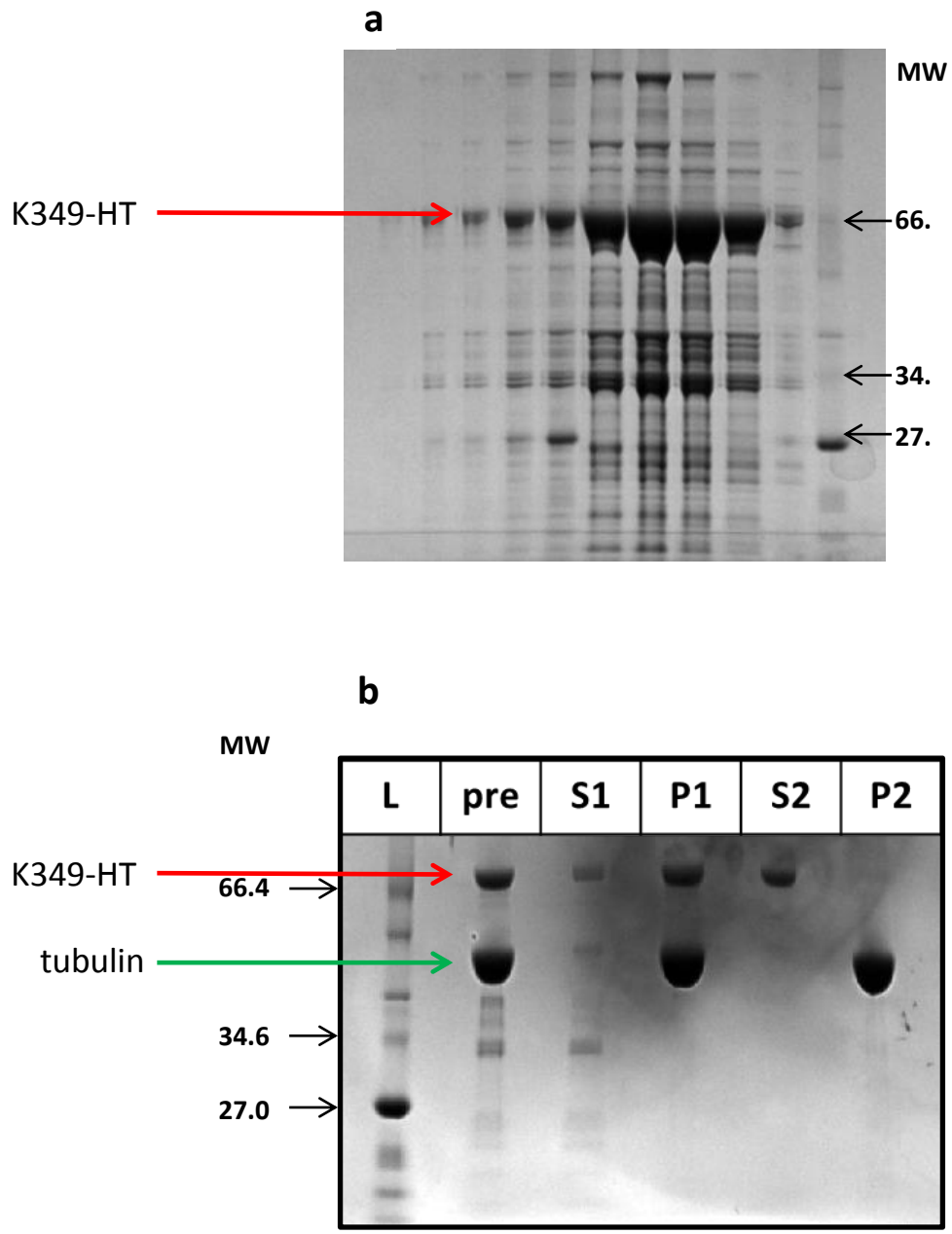

Figure 2.13. Protein gel and MTBR results of K349-HT
a) A protein gel was run to verify results of K349-HT protein expression. Molecular weight is 71609 g/mol and extinction coefficient is 86978 cm^{-1} M^{-1}. **b)** Purification was done by MTBR, where L: protein ladder, pre: MT and motor mixture, S1: Supernatant with inactive motors, P1: MT with active motors bound, S2: Recovered active motors used in the rest of the study, P2: MT after separation from motor

2.3.1.5. DNA Labeling of K349-HT

Attachment of the K349-HT monomers to beads in the optical trap assay has been done with the same double stranded DNA used for K349-E215C binding, but using a different crosslinker between the monomer and the DNA. The HaloTag protein that was inserted into the kinesin monomer provides easy attachment to a HalotTag ligand, in this case an NHS-HaloTag ligand that binds the monomer via the ligand and the DNA via the NHS-amine reaction.

For DNA labeling, oligos have been hybridized as before and incubated with 40x excess of HaloTag succinimidyl ester ligand (Promega) at room temperature for 6 hours. The reaction was quenched by adding 1mM glycine to the solution. Excess HaloTag was removed by desalting through Illustra MicroSpin G-25 columns twice. The resulting DNA-HT ligand was then mixed with K349-HT and reacted overnight at 4 ˚C. Labeling has been verified by running a gel and labeling two different ways as before, and results are shown in Figure 2.14.

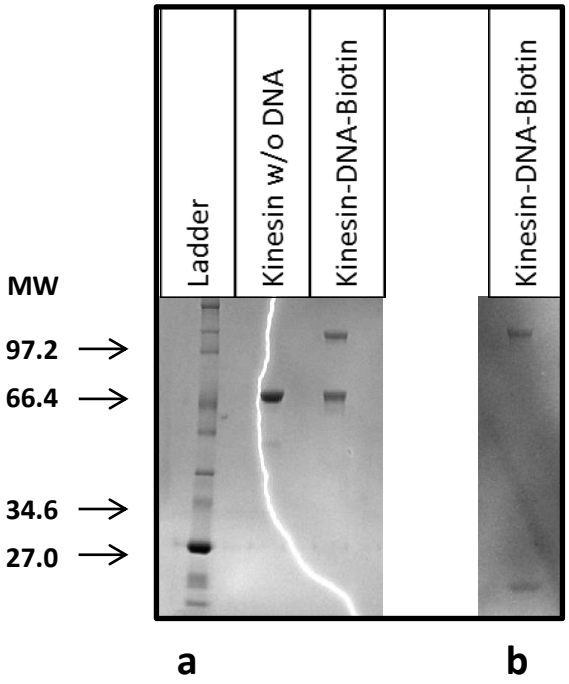

Figure 2.14. DNA-Labeling of K349-HT
a) Protein gel is run and then stained with coomassie. Here, ladder is in the first lane, unlabeled K349-HT in the second lane and K349-HT-DNA in the third lane. The labeled product has a higher molecular weight as expected and there is an almost equal amount of unlabeled K349-HT left in the solution. b) Second half of the gel (with the same set of solutions) is labeled with methylene blue, where only the product K349-HT-DNA is visible at the same height as in the first half of the gel. (There is also some excess DNA in this lane)

2.3.2. Preparation of dynein

We have prepared Alexa488-labeled *S. cerevisiae* cytoplasmic dynein molecules to aid in polarity determination of axonemes in the optical trap experiments by accumulating at the minus end. Dyneins with HaloTag were prepared as described elsewhere [42], and labeled with an Alexa488 HaloTag ligand.

2.4. Optical trap assay

2.4.1. Sample Preparation

For the optical trap assay, DNA labeled kinesin monomers are diluted (between 100,000 to 1,000,000 fold) in BRBC (kinesin assay buffer BRB80 with 2.5 mg/ml casein, BRB80 = 80 mM PIPES, 1 mM $MgCl_2$, 1 mM EGTA, pH 6.8). This dilution ensures that we will see only single stepping events and rarely multiple steps in a single oscillation of the bead that would imply the presence of multiple motors on a bead. We do not observe any events in the absence of the motor. Streptavidin beads (860 nm, Invitrogen) are diluted 10x from stock, and sonicated for 10 seconds. 5 μl of motor solution is mixed with 5 μl of beads by pipetting gently, and reacted on ice for 10 minutes.

A chamber is made by binding a coverslip on top of a microscope slide with double-sided tape on two edges, forming a channel for flowing in solutions Figure 2.15a. Cy5 labeled axonemes are diluted in dynein loading buffer (DLB = 30 mM HEPES, 2 mM $MgCl_2$, 1 mM EDTA, 10% glycerol, pH 7.2) to a concentration where their distribution on the surface by non-specific binding is sparse enough when observed in a 633 nm laser TIRF channel. The channel is then washed with 30 μl DLB, followed by 20 μl DLBC (DLB with 1mg/ml casein and 2 mM DTT). Alexa488 labeled dyneins are diluted in DLBC and introduced into the channel. After a minute, unbound dyneins are rinsed with 20 μl DLBC. 20 μl of 20 μM ATP in DBLC is flown in to set dyneins into motion towards the minus end of the axonemes where they accumulate and serve as polarity markers (Figure 2.15b). ATP is then rinsed out five times with 20 μl DLBC and once with 30 μl BRBC.

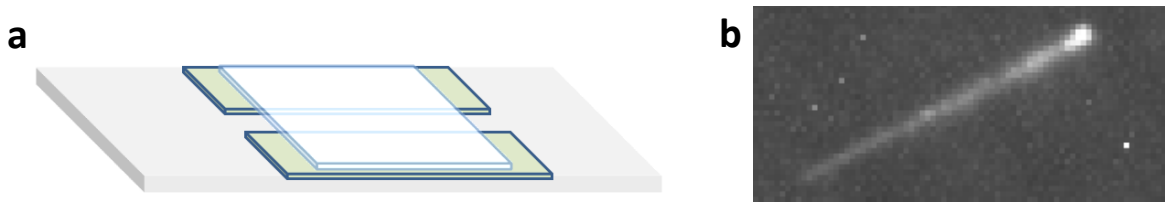

Figure 2.15. Flow channels and Alexa488 labeled dyneins on an axoneme
a) A flow chamber is formed by taping a coverslip on a microscope slide from two edges with double sided tape. The area between the tapes is the channel where solutions are flown through. **b)** Dyneins walk towards the minus end of the axoneme and accumulate there. This helps to determine the polarity of the axoneme. 488 labeled dyneins are observed in a 532 nm TIRF channel.

The motor solution contains some residual ATP from MTBR purification. To remove the residual ATP, the bead-motor mixture is further diluted by adding 200 µl of BRBC and spinning on a tabletop spinner for 90 seconds and discarding the supernatant. This is repeated once more and the supernatant is removed leaving a bead-motor solution of ~ 2 µl. This solution is diluted 10x in a specific stepping buffer according to the nucleotide conditions tested in the experiment, and the final bead-motor-nucleotide solution is introduced into the chamber. The chamber is then sealed on both ends with clear nail polish with very low auto-fluorescence. The stepping buffers are BRB80 containing a PCD/PCA oxygen scavenging system, DTT, 1 mg/ml casein and according to the nucleotide conditions tested, the reagents listed in Table 2.1.

Conditions	Nucleotide	Additional Reagents	Reason
ATP	1 mM ATP		
ADP	1 mM ADP	2 U/ml Hexokinase 0.4 % Glucose	to convert leftover ATP into ADP
No nucleotide		0.5 U/ml Apyrase	to consume leftover ATP

Table 2.1. Contents of stepping buffers according to nucleotide conditions
Additional reagents added to the stepping buffer are listed for each nucleotide condition.

2.4.2. Optical Trapping and Data Collection

Once, the chamber is mounted on the optical trap system, a surface-attached Cy5-labeled axoneme oriented parallel is chosen using the 633 nm TIRF channel. The 532 nm TIRF channel is next used to determine the axoneme polarity with surface bound dynein motors, which accumulate at the minus end tip of axonemes. After determination of the microtubule polarity, a freely diffusing monodisperse bead is trapped and positioned over the axoneme. We oscillate the bead 125 nm in forward and reverse directions along the axoneme and hold for .375

seconds in each position. If a motor on the bead binds the microtubule, it will hinder the oscillating bead from fully following the trap center until released from the microtubule either by the forces exerted by the optical trap or by ATP hydrolysis. An exemplary case is shown in Figure 2.16a. During the experiment the traces of the bead and trap centers are recorded at 20 kHz by custom software written in LabView. Figure 2.16b shows the traces where one can see the oscillation of the trap (green) between ± 125 nm, in this case with a period of 0.5 seconds. The bead center follows the trap center. However, when a motor on the bead binds to the axoneme during oscillation (1), it will hinder the bead from reaching the trap center (2) and the monomer experiences tension depending on the bead-trap separation. When the monomer releases from the microtubule, and the bead will immediately return to the trap center (3). This event is step-fitted by finding the separation between the bead and trap center, and the time it took for the kinesin to release (Figure 2.16c). The stiffness of the optical trap, which is typically between 0.4 and 0.6 in our system, was calibrated by finding the corner frequency of bead oscillation by Lorentzian fitting. The force exerted by trap is calculated by the Hooke's Law.

Another unique feature of our assay is that we can record many events in one experiment and rapidly collect sufficient data for statistical analysis.

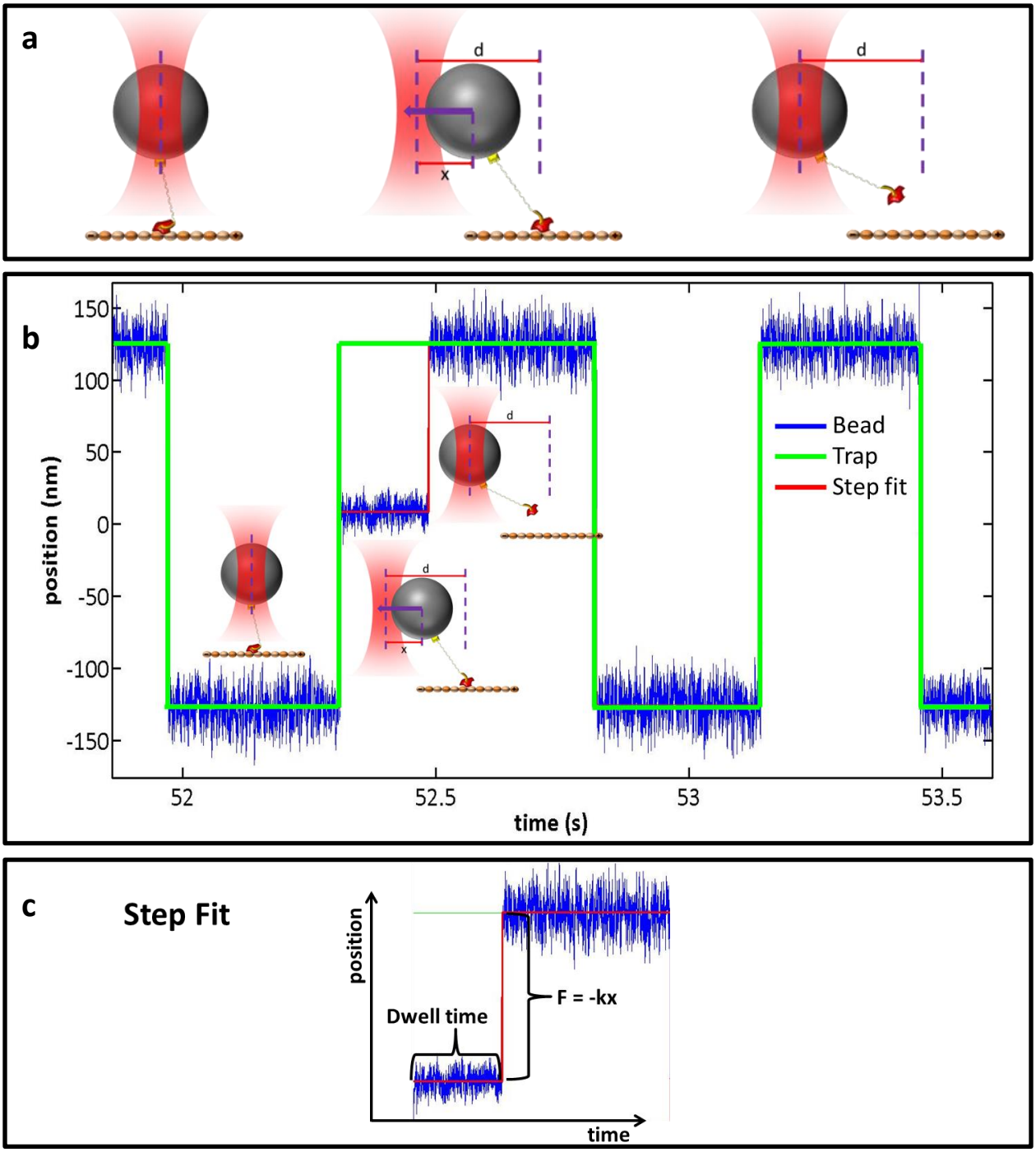

Figure 2.16. Forced release of trapped kinesin monomers from microtubules
a) 1-A kinesin monomer on the trapped bead binds the microtubule. **2-**Trap oscillation forces the bead to move to a new position on a microtubule, but the bound kinesin hinders the bead from following the trap. **3-**Upon release of the kinesin from the microtubule, bead keeps up with the trap. **b)** Recorded traces of the bead center (blue) and trap center (green) show the above event. The centers overlap during oscillation except when a bound kinesin hinders the bead from fully following the trap (2). The bead stays at another equilibrium position until the kinesin releases from the MT and the bead can return to the trap center (3). **c)** The trace is fitted by a step finder. The force is calculated by Hooke's law where the distance is the separation between bead and trap centers.

2.4.3. Advantages of the new trapping assay

Monitoring the release of a monomer from microtubules, at constant forces and linker orientations is a direct measurement of the gating models. By providing this ability, our optical trap assay offers many advantages over previous designs.

The most relevant study to our work was done by Uemura et el. [43] where they optically trapped kinesin monomers. By moving the trap at a constant velocity, they measured the abrupt rupture force of a monomer from its track in the instant of dissociation (Figure 2.17). In this setup, the force that the monomer feels is constantly increasing and depends on the velocity of the trap, and hence on experimental conditions. This rupture force is not a reliable parameter to understand the actual release behavior of kinesin, since it does not represent the tension the heads of a walking dimer may experience during stepping. During a release event, we expect a constant tension on the monomer, as opposed to a constantly increasing tension. These experiments are thus unsuitable for accurate determination of how fast a head releases microtubules under tension.

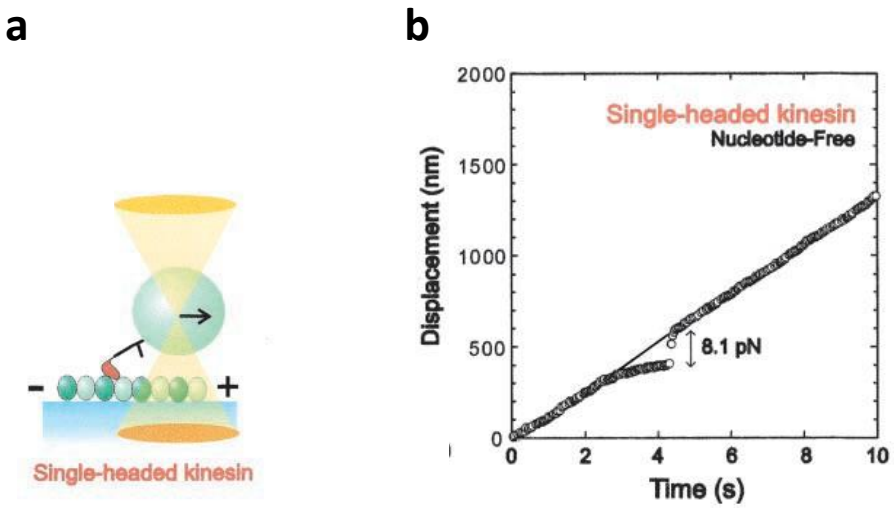

Figure 2.17. Relevant experiments
a) Illustration of a kinesin monomer bound to a bead in an optical trap where the bead moves with constant velocity. **b)** Abrupt rupture of the monomer from the microtubule in a displacement vs time plot. The force corresponds to the pulling force at the instance of rupture. (Figures from [43])

In our trap assay, a release event happens as depicted in Figure 2.16a. The bead moves with the trap until a monomer on the bead attaches to the microtubule. From the onset of the attachment, the bead cannot follow the trap and the bead center will be separated a certain distance from the trap center. The monomer will experience a constant tension in this geometry until it releases from the microtubule, upon which the bead instantly returns to the trap center. So, each release event we observe has a known tension and dwell time which is a significant improvement compared to previous motor unbinding assays.

Another advantage worth mentioning is the large number of events we observe which is in thousands compared to the limited events that were reported in the other study with a maximum of 63 events for a case studied.

The reliable representation of events and the large data sets give us the ability to directly observe and statistically analyze dwell times of kinesin under a large range of constant forces, from which we can directly calculate kinesin release rate from microtubules and provide a direct examination of gating.

2.4.4. Data Analysis

The traces collected in LabView and trap stiffness parameters have been fed into a custom written Matlab code that fits the steps to the traces and produces images and measurements of each stepping event (Figure 2.16c). Each of these images is then checked visually to discard any misfits or rare events with multiple steps. For the approved stepping events, the force is calculated according to trap stiffness and the direction kinesin steps towards to separate assistive versus resistive force depending on stepping towards the plus or minus end of the axoneme. Force versus dwell time information is then binned to average over a force and fitted into a double exponential in Origin. The higher of the time parameters is accepted as average dwell time parameter. In a separate analysis, events shorter than 5 ms were excluded from the data analysis, and the histogram was fitted to a single exponential. Similar parameters were obtained by this alternative method (the results are not shown). Finally, release rate is plotted against average force in each bin.

Sample Double Exponential Fits to Data

	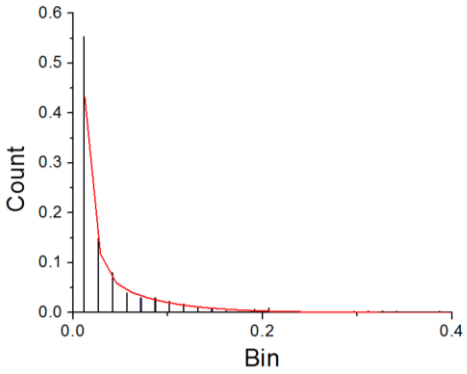	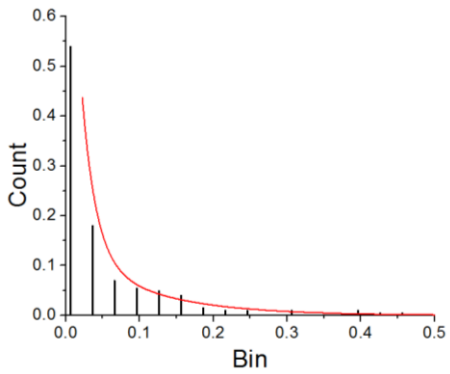
Condition	Head ADP forward (bin 300)	Linker ATP backward (bin 200)
Fit bin size	.015	0.03
Avg force (pN)	3.6036	-1.8640
k (1/s)	17.80627	9.539254

	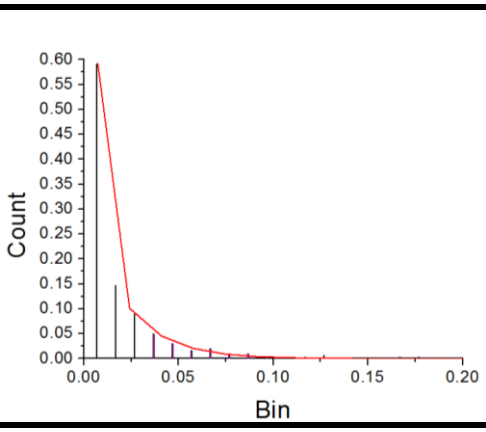	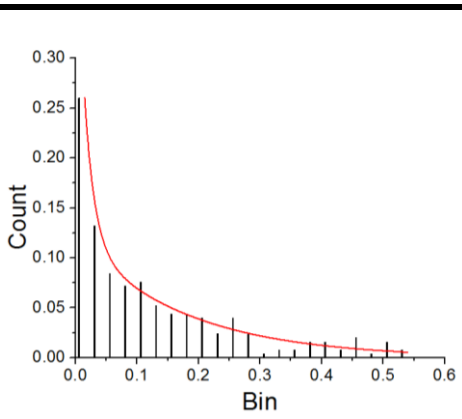
Condition	Head ADP backward (bin 300)	Linker ADP backward (bin 250)
Fit bin size	.01	0.025
Avg force (pN)	8.9711	-2.07009
k (1/s)	47.37091	5.396363

Figure 2.18. Sample Double Exponential Fits to Data
Sample fits in different conditions. Bin size in parenthesis represents initial partition of the data points into bins. Bin sizes used for fitting each partition are shown along with the average force and obtained time parameter.

2.5. References

[1] A. Ashkin, “Acceleration and Trapping of Particles by Radiation Pressure,” *Phys. Rev. Lett.*, vol. 24, no. 4, pp. 156–159, Jan. 1970.

[2] A. Ashkin and J. M. Dziedzic, “Optical Levitation by Radiation Pressure,” *Appl. Phys. Lett.*, vol. 19, no. 8, pp. 283–285, Oct. 1971.

[3] A. Ashkin, J. M. Dziedzic, J. E. Bjorkholm, and S. Chu, “Observation of a single-beam gradient force optical trap for dielectric particles,” *Opt. Lett.*, vol. 11, no. 5, pp. 288–290, May 1986.

[4] K. C. Neuman and S. M. Block, “Optical trapping,” *Rev. Sci. Instrum.*, vol. 75, no. 9, pp. 2787–2809, Sep. 2004.

[5] K. Svoboda and S. M. Block, “Biological Applications of Optical Forces,” *Annu. Rev. Biophys. Biomol. Struct.*, vol. 23, no. 1, pp. 247–285, 1994.

[6] R. Simmons, “Molecular motors: Single-molecule mechanics,” *Curr. Biol.*, vol. 6, no. 4, pp. 392–394, Apr. 1996.

[7] S. Khan and M. P. Sheetz, “Force Effects on Biochemical Kinetics,” *Annu. Rev. Biochem.*, vol. 66, no. 1, pp. 785–805, 1997.

[8] C. M. Coppin, D. W. Pierce, L. Hsu, and R. D. Vale, “The load dependence of kinesin’s mechanical cycle,” *Proc. Natl. Acad. Sci.*, vol. 94, no. 16, pp. 8539–8544, Aug. 1997.

[9] M. W. Allersma, F. Gittes, M. J. deCastro, R. J. Stewart, and C. F. Schmidt, “Two-Dimensional Tracking of ncd Motility by Back Focal Plane Interferometry,” *Biophys. J.*, vol. 74, no. 2, pp. 1074–1085, Feb. 1998.

[10] M. D. Wang, “Manipulation of single molecules in biology,” *Curr. Opin. Biotechnol.*, vol. 10, no. 1, pp. 81–86, Feb. 1999.

[11] K. Visscher, M. J. Schnitzer, and S. M. Block, “Single kinesin molecules studied with a molecular force clamp,” *Nature*, vol. 400, no. 6740, pp. 184–189, Jul. 1999.

[12] A. D. Mehta, M. Rief, J. A. Spudich, D. A. Smith, and R. M. Simmons, “Single-Molecule Biomechanics with Optical Methods,” *Science*, vol. 283, no. 5408, pp. 1689–1695, Mar. 1999.

[13] I. Crevel, N. Carter, M. Schliwa, and R. Cross, “Coupled chemical and mechanical reaction steps in a processive Neurospora kinesin,” *EMBO J.*, vol. 18, no. 21, pp. 5863–5872, Nov. 1999.

[14] C. Bustamante, J. C. Macosko, and G. J. L. Wuite, “Grabbing the cat by the tail: manipulating molecules one by one,” *Nat. Rev. Mol. Cell Biol.*, vol. 1, no. 2, pp. 130–136, Nov. 2000.

[15] K. Kawaguchi and S. Ishiwata, “Temperature Dependence of Force, Velocity, and Processivity of Single Kinesin Molecules,” *Biochem. Biophys. Res. Commun.*, vol. 272, no. 3, pp. 895–899, Jun. 2000.

[16] S. C. Kuo, “Using Optics to Measure Biological Forces and Mechanics,” *Traffic*, vol. 2, no. 11, pp. 757–763, 2001.

[17] A. Ishijima and T. Yanagida, “Single molecule nanobioscience,” *Trends Biochem. Sci.*, vol. 26, no. 7, pp. 438–444, Jul. 2001.

[18] Y. Ishii, A. Ishijima, and T. Yanagida, “Single molecule nanomanipulation of biomolecules,” *Trends Biotechnol.*, vol. 19, no. 6, pp. 211–216, Jun. 2001.
[19] K. Kawaguchi and S. Ishiwata, “Nucleotide-Dependent Single- to Double-Headed Binding of Kinesin,” *Science*, vol. 291, no. 5504, pp. 667–669, Jan. 2001.
[20] R. Mallik, B. C. Carter, S. A. Lex, S. J. King, and S. P. Gross, “Cytoplasmic dynein functions as a gear in response to load,” *Nature*, vol. 427, no. 6975, pp. 649–652, Feb. 2004.
[21] S. M. Block, L. S. B. Goldstein, and B. J. Schnapp, “Bead movement by single kinesin molecules studied with optical tweezers,” *Nature*, vol. 348, no. 6299, pp. 348–352, Nov. 1990.
[22] A. Yildiz, M. Tomishige, A. Gennerich, and R. D. Vale, “Intramolecular Strain Coordinates Kinesin Stepping Behavior along Microtubules,” *Cell*, vol. 134, no. 6, pp. 1030–1041, Sep. 2008.
[23] K. Svoboda, C. F. Schmidt, B. J. Schnapp, and S. M. Block, “Direct observation of kinesin stepping by optical trapping interferometry,” *Nature*, vol. 365, no. 6448, pp. 721–727, Oct. 1993.
[24] J. T. Finer, R. M. Simmons, and J. A. Spudich, “Single myosin molecule mechanics: piconewton forces and nanometre steps,” *Nature*, vol. 368, no. 6467, pp. 113–119, Mar. 1994.
[25] J. Liphardt, B. Onoa, S. B. Smith, I. Tinoco, and C. Bustamante, “Reversible Unfolding of Single RNA Molecules by Mechanical Force,” *Science*, vol. 292, no. 5517, pp. 733–737, Apr. 2001.
[26] X. Zhuang, “Single-Molecule Rna Science,” *Annu. Rev. Biophys. Biomol. Struct.*, vol. 34, no. 1, pp. 399–414, 2005.
[27] I. Tinoco, P. T. X. Li, and C. Bustamante, “Determination of thermodynamics and kinetics of RNA reactions by force,” *Q. Rev. Biophys.*, vol. 39, no. 04, pp. 325–360, 2006.
[28] C. Cecconi, E. A. Shank, C. Bustamante, and S. Marqusee, “Direct Observation of the Three-State Folding of a Single Protein Molecule,” *Science*, vol. 309, no. 5743, pp. 2057–2060, Sep. 2005.
[29] D. E. Smith, S. J. Tans, S. B. Smith, S. Grimes, D. L. Anderson, and C. Bustamante, “The bacteriophage φ29 portal motor can package DNA against a large internal force,” *Nature*, vol. 413, no. 6857, pp. 748–752, Oct. 2001.
[30] C. Bustamante, Z. Bryant, and S. B. Smith, “Ten years of tension: single-molecule DNA mechanics,” *Nature*, vol. 421, no. 6921, pp. 423–427, Jan. 2003.
[31] J. R. Moffitt, Y. R. Chemla, S. B. Smith, and C. Bustamante, “Recent Advances in Optical Tweezers,” *Annu. Rev. Biochem.*, vol. 77, no. 1, pp. 205–228, 2008.
[32] S. S. Rosenfeld, J. Xing, G. M. Jefferson, H. C. Cheung, and P. H. King, “Measuring Kinesin’s First Step,” *J. Biol. Chem.*, vol. 277, no. 39, pp. 36731–36739, Sep. 2002.
[33] “Optical tweezers,” *Wikipedia, the free encyclopedia*. 27-Jul-2013.
[34] J. W. Shaevitz, “A Practical Guide to Optical Trapping,” 22-Aug-2006. [Online]. Available: http://genomics.princeton.edu/shaevitzlab/OT_Practicle_Guide.pdf.
[35] K. Neuman, E. Chadd, G. Liou, K. Bergman, and S. Block, “Characterization of photodamage to escherichia coli in optical traps,” *Biophys. J.*, vol. 77, no. 5, pp. 2856–2863, Nov. 1999.

[36] “Single molecule measurements and biological motors.” [Online]. Available: http://www2.bioch.ox.ac.uk/oubsu/ebjknight/title.html. [Accessed: 07-Aug-2013].
[37] G. D. Reddy and P. Saggau, “Fast three-dimensional laser scanning scheme using acousto-optic deflectors,” *J. Biomed. Opt.*, vol. 10, no. 6, pp. 064038–064038–10, 2005.
[38] “Nikon MicroscopyU | Fluorescence Microscopy | TIRF Basics.” [Online]. Available: http://www.microscopyu.com/articles/fluorescence/tirf/tirfintro.html. [Accessed: 09-Aug-2013].
[39] S. Rice, A. W. Lin, D. Safer, C. L. Hart, N. Naber, B. O. Carragher, S. M. Cain, E. Pechatnikova, E. M. Wilson-Kubalek, M. Whittaker, E. Pate, R. Cooke, E. W. Taylor, R. A. Milligan, and R. D. Vale, “A structural change in the kinesin motor protein that drives motility,” *Nature*, vol. 402, no. 6763, pp. 778–784, Dec. 1999.
[40] M. Tomishige, N. Stuurman, and R. D. Vale, “Single-molecule observations of neck linker conformational changes in the kinesin motor protein,” *Nat. Struct. Mol. Biol.*, vol. 13, no. 10, pp. 887–894, Oct. 2006.
[41] I. R. Gibbons, J. E. Garbarino, C. E. Tan, S. L. Reck-Peterson, R. D. Vale, and A. P. Carter, “The Affinity of the Dynein Microtubule-binding Domain Is Modulated by the Conformation of Its Coiled-coil Stalk,” *J. Biol. Chem.*, vol. 280, no. 25, pp. 23960–23965, Jun. 2005.
[42] S. L. Reck-Peterson, A. Yildiz, A. P. Carter, A. Gennerich, N. Zhang, and R. D. Vale, “Single-Molecule Analysis of Dynein Processivity and Stepping Behavior,” *Cell*, vol. 126, no. 2, pp. 335–348, Jul. 2006.
[43] S. Uemura, K. Kawaguchi, J. Yajima, M. Edamatsu, Y. Y. Toyoshima, and S. Ishiwata, “Kinesin–microtubule binding depends on both nucleotide state and loading direction,” *Proc. Natl. Acad. Sci.*, vol. 99, no. 9, pp. 5977–5981, Apr. 2002.

Chapter 3. Results for Force Response of Kinesin Monomers

3.1. Experimental reasoning and hypothesis

We designed our experiments to differentiate between the responses of kinesin monomers to load in two situations as illustrated in Figure 3.1a. First, we pulled kinesin from the head domain when the neck-linker is free. These measurements allow determination of the force-induced release rate of the kinesin head from MTs in both directions. Second, we pulled kinesin from its neck-linker to test gating models based on neck-linker orientation, discussed in Chapter 1. Both these cases are studied under three different nucleotide conditions to reveal the force response mechanism of kinesin. These conditions are saturating ATP conditions, saturating ADP conditions and absence of any nucleotide (apo).

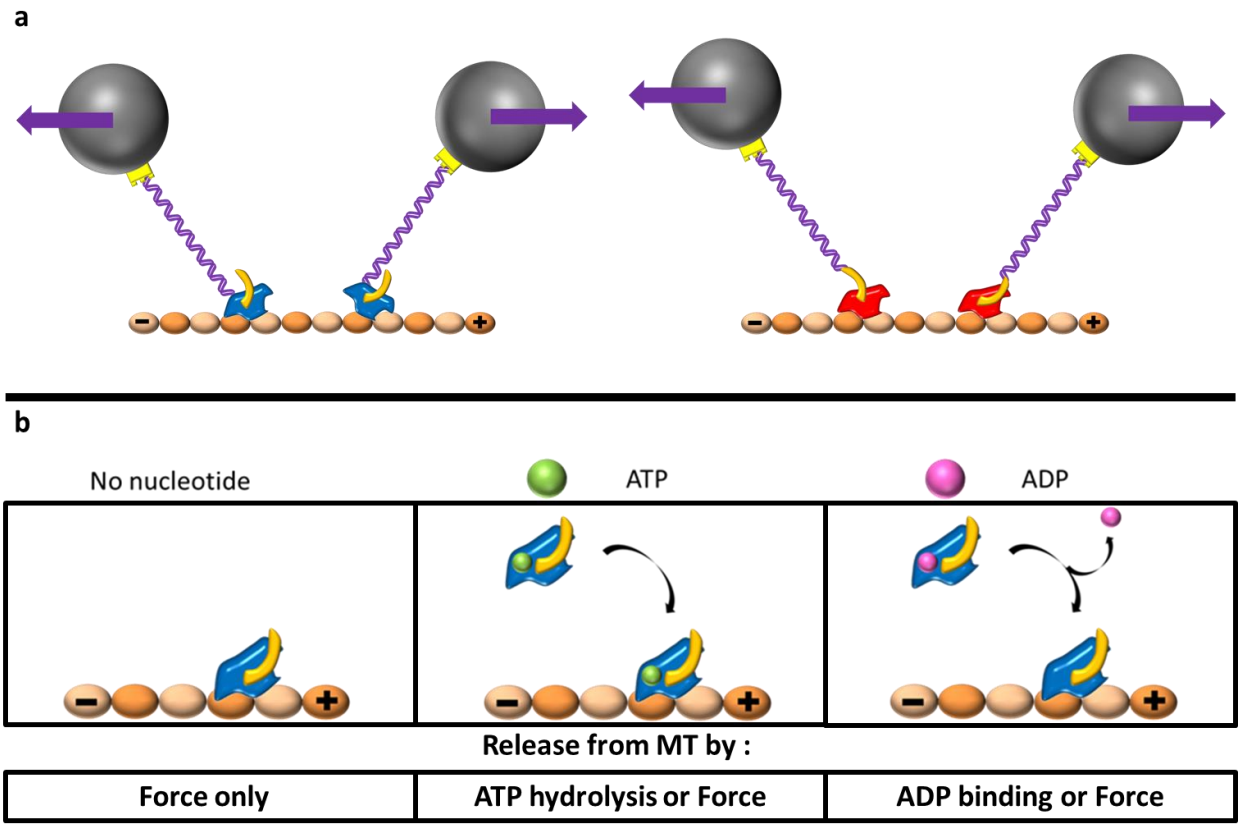

Figure 3.1. Nucleotide conditions tested in the optical trap experiments
a) Representations of head-bound monomer (blue) and linker-bound monomer (red) being pulled forward or backwards. **b)** Under *apo* conditions, the microtubule-bound monomer has no nucleotide and will only be released by the force from the trap. Under *saturating ATP* conditions, the microtubule-bound monomer may have an ATP when bound. It can release by hydrolysis or by the trap force. Under *saturating ADP* conditions, the microtubule-bound monomer has no nucleotide. It can release upon binding an ADP or by trap force.

In the absence of a nucleotide (apo) (Figure 3.1b), kinesin monomers stably bind the microtubule and do not spontaneously release on their own at a short timescale. The only possibility to see a fast release event in this case is when the load exerted by trap on the monomer detaches it from the microtubule. Since detachment is only force dependent, we expect to observe release properties, regardless of where the load was exerted on kinesin monomers (e.g. pulling from the head or the linker). This condition is therefore a necessary control for the comparison of the two constructs.

Under saturating ADP conditions, we expect to see a difference in release properties between the two constructs if the linker is indeed involved in gating nucleotide binding. When a free kinesin monomer binds ADP in solution, it must release its ADP upon microtubule attachment (Figure 3.1b). Therefore, we expect the monomers to be in a nucleotide free state when they bind to microtubule. Once pulled with optical trap, there can be two possible causes for a release event. The monomers can release under load exerted force from the trap, similar to the apo condition. Alternatively, ADP binding to the head can mimic its release from the microtubule irrespective of the applied load. When kinesin is pulled through the head region, the neck linker dynamics is not altered. Therefore, addition of ADP should increase the microtubule release rate irrespective of the direction and magnitude of the applied load. When kinesin is pulled from its linker, one can expect to see two different situations if the neck-linker orientation is critical for nucleotide binding to the head. According to this possibility, if the load is towards the forward direction, this case resembles the rear head of a kinesin dimer, which is in an on state and free to bind a nucleotide. Pulling on the linker in this direction should therefore not greatly influence nucleotide binding and show results similar to above cases. The crucial situation we investigate however is when we are pulling on the linker rearward, and simulating the front head of a kinesin dimer. The front head of a microtubule bound dimer is in an off-state where it cannot bind ATP. If a front head gating is in place, we expect to observe slower release under backward load, in comparison to the monomers under forward load (Figure 3.2a). If the trap mimics the fully gated state of the linker under backward load, we may observe release properties similar to the apo conditions towards this direction.

Under saturating ATP conditions, it is possible for a kinesin monomer to bind an ATP while floating free in the solution. Because kinesin binds strongly to microtubule in its ATP state, it can keep its ATP during microtubule attachment (Figure 3.1b). In the event that an ATP is already bound to the monomer when we are manipulating it with the trap, it is not possible to observe the linkers involvement in nucleotide binding. In this condition, it is therefore possible to observe two kinds of microtubule release events. One that is driven by ATP hydrolysis or one that is caused by the tension from the trap. We expect this case to again have a similar outcome when kinesin is pulled from the neck linker, provided that the neck-linker does not interfere with ATP hydrolysis. However, if an assistive rear head gating is in place, and if the linker orientation is critical for nucleotide release, we then expect to see similar asymmetry described above for the ADP conditions, such that the monomers release faster when pulled forward than backward in the presence of ATP (Figure 3.2b).

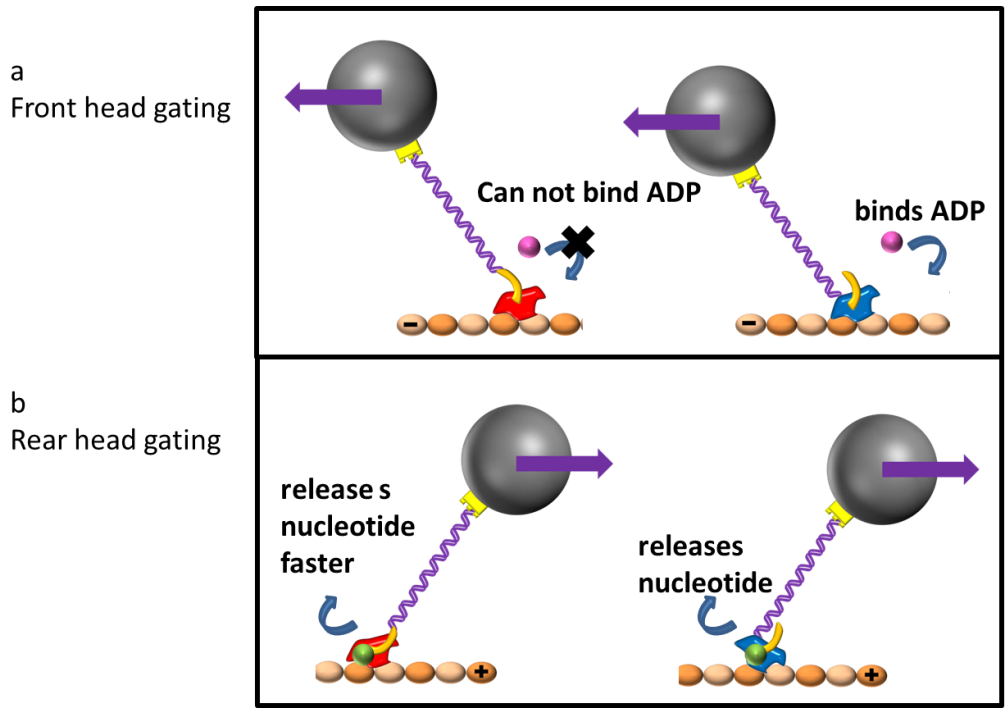

Figure 3.2. Hypothesis for gating
a) If there is front head gating, in saturating ADP conditions, linker-pulled construct will not bind ADP when pulled backwards, whereas the head-pulled construct will be able to freely bind ADP. **b)** If there is rear head gating, in saturating ATP conditions, linker-pulled will release nucleotide faster than the head-pulled construct.

A complete representation of experiments and possible release mechanisms are shown for head-pulled construct and linker-pulled construct in Figure 3.3 and Figure 3.4 respectively.

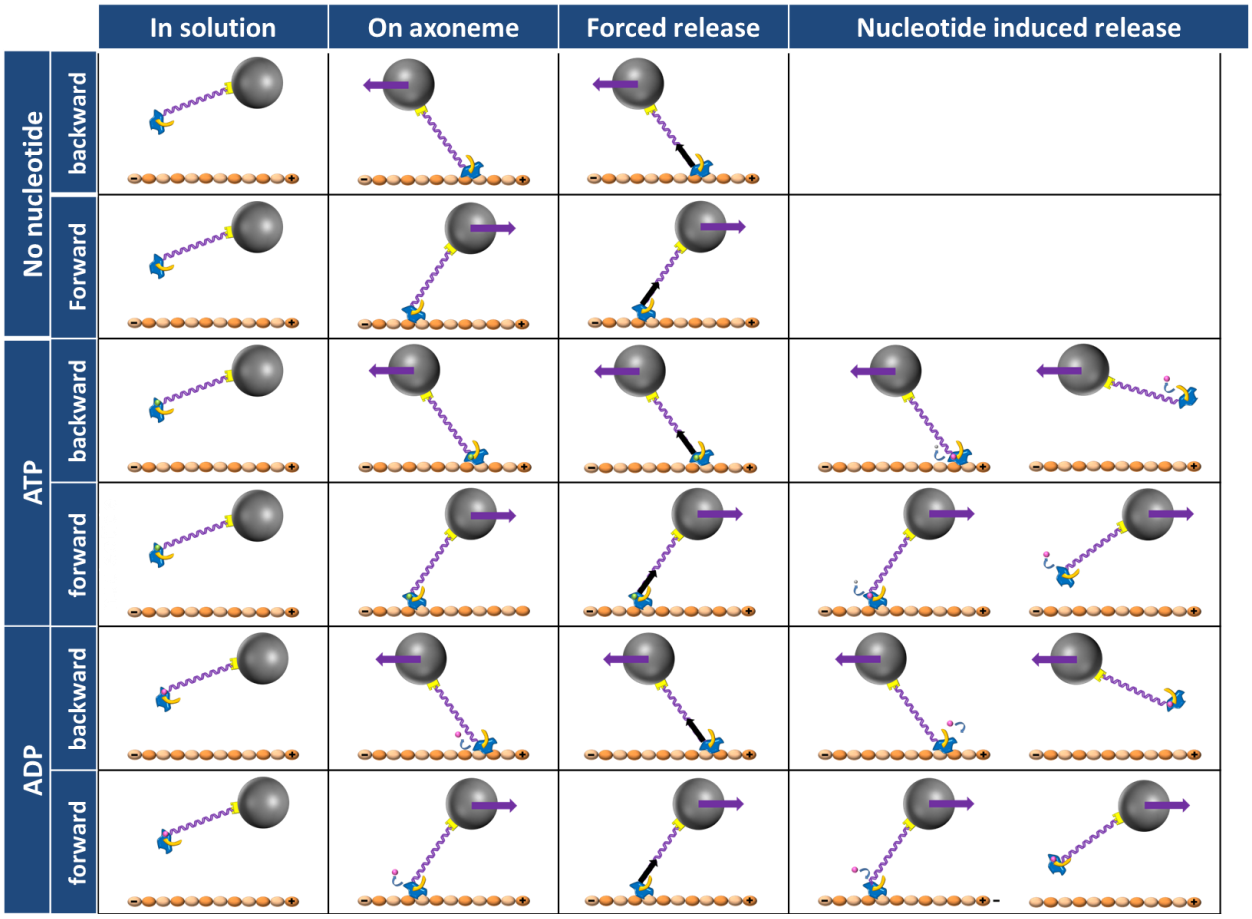

Figure 3.3. Representation of experiments for head-bound monomer
In solution, monomers can bind nucleotides, however only ATP can remain bound on the microtubule. Monomers can be released by force in all conditions and in both directions. ATP bound monomers can also release by hydrolysis. In ADP conditions, monomers can release if they bind ADP.

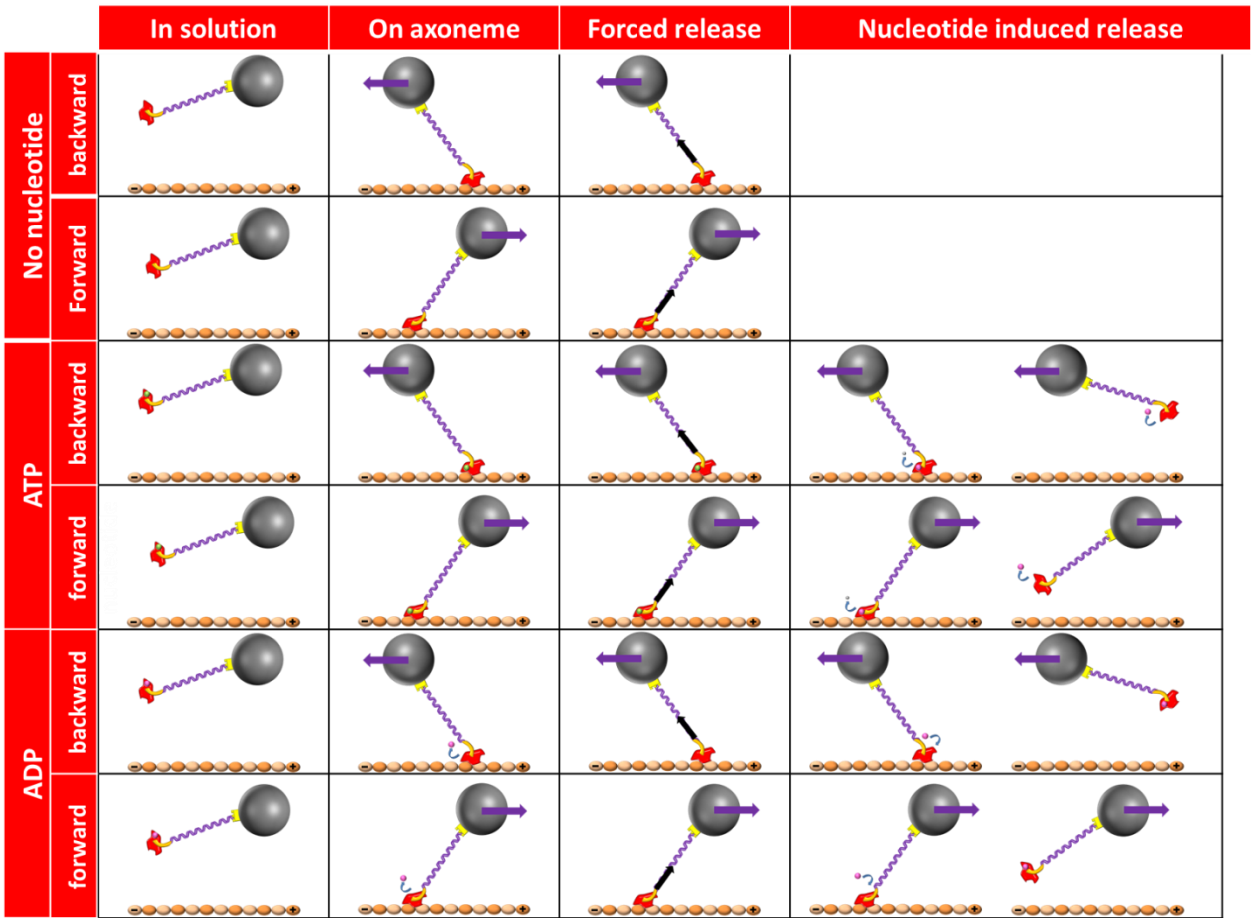

Figure 3.4. Representation of experiments for linker-bound monomer
In solution, monomers can bind nucleotides, however only ATP can remain bound on the microtubule. Monomers can be released by force in all conditions and in both directions. ATP bound monomers can also release by hydrolysis. In ADP conditions, monomers can release if they bind ADP.

3.2. Results

Results are plotted as release rate of a monomer from the microtubule versus average force. Plus-end directed forces that are assistive for the directionality of kinesin motility are marked as positive forces, and resistive forces towards the minus end are marked as negative forces. Average forces are calculated by binning the data into a pre-set bin size that varies for each case depending on the number of data points collected. Release rate at a given force is found by fitting the dwell times into an exponential decay. Error bars in the graphs are calculated from the standard error of the fits.

3.2.1. Results for head-pulled kinesin monomer

Results for the nucleotide induced load responses of the head-pulled construct are shown in Figure 3.5. ATP conditions show significantly higher release rates compared to apo conditions in agreement with our expectations for rapid release by ATP hydrolysis. There is no asymmetry between release rates in either direction, indicating that the kinesin monomer doesn't have a strong preference for release from microtubule in a particular direction. ADP conditions show a similar behavior to ATP conditions and have a slightly lower release rate and possibly a slightly smaller affinity for kinesin. Similarities between the ATP and ADP conditions prove that the region where we pull from on the head does not interfere with nucleotide binding either. Release rates increase with force for all cases.

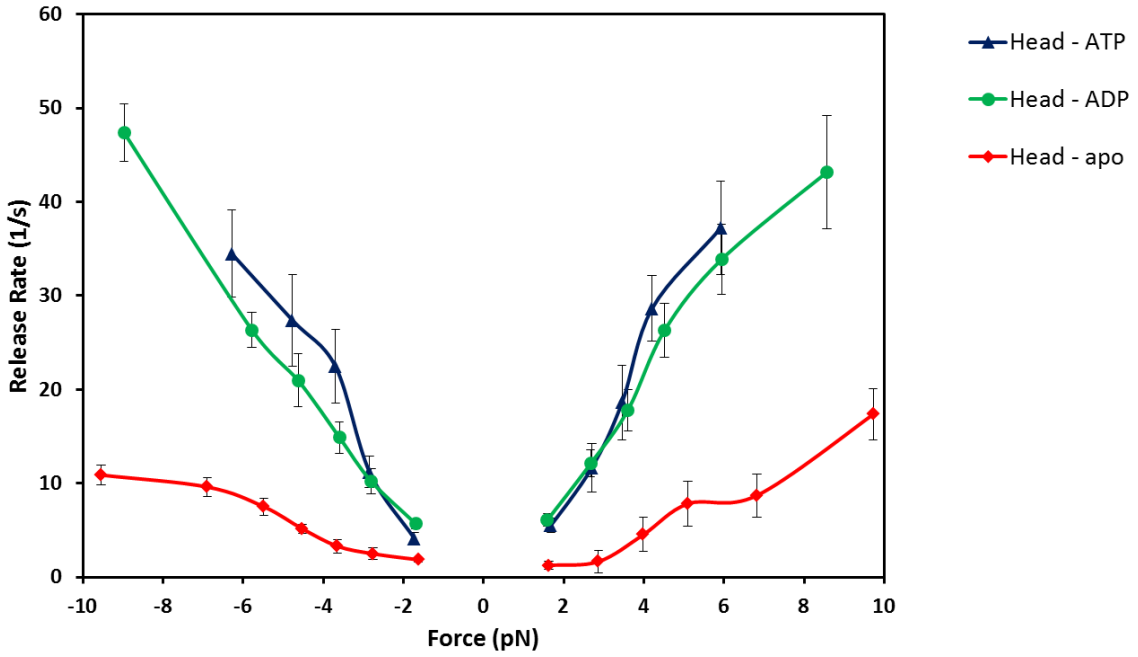

Figure 3.5. Nucleotide induced load responses of the head-pulled kinesin monomer construct
Release rates under different nucleotide conditions are shown for head pulled construct (Head), where ATP, ADP and apo conditions are plotted blue, green and red respectively.

3.2.1.1. The Release Rate in the apo Condition Increases under Force in both Directions

The apo condition for the head-pulled monomer helps us determine the rate of microtubule release when the motor can only detach from microtubule under load. We observed that the rate is low (1 s^{-1}) under a low load regime (1-2 pN) and increases progressively to 10 s^{-1} at forces higher than 6 pN. There is no strong asymmetry between the backwards release rate plot and forward release plot (Figure 3.6). Figure 3.6 reveals that detaching a monomer requires

comparable amounts of load in both directions. The release towards the plus end is slightly higher at large forces.

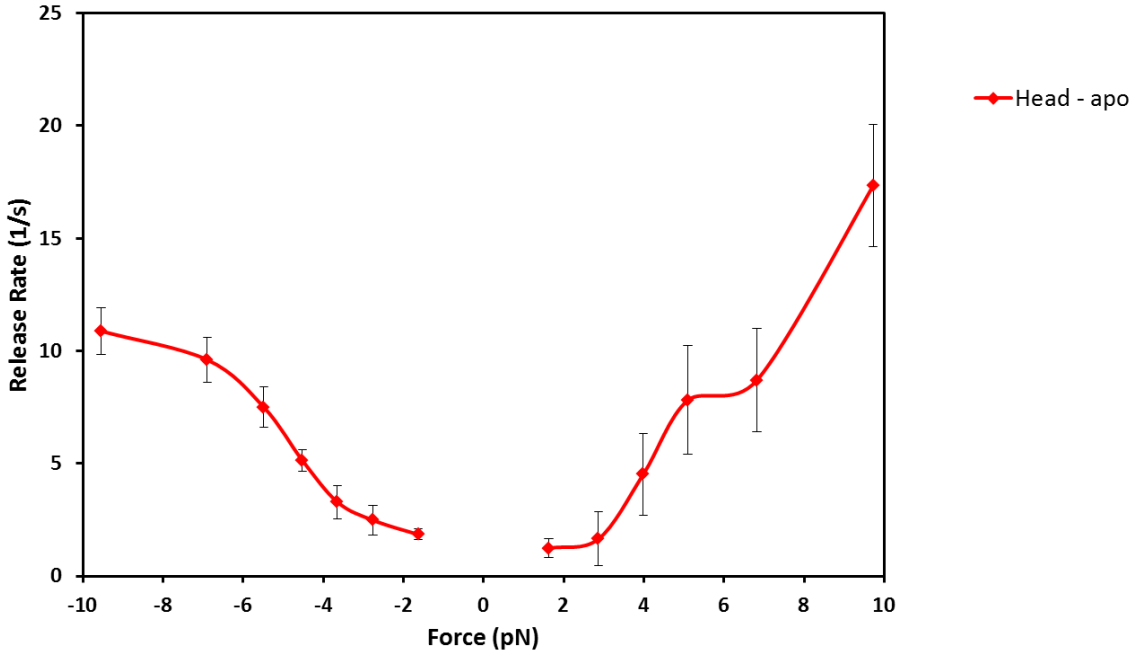

Figure 3.6. The release rate under no nucleotide conditions
In the absence of nucleotide, there is no strong asymmetry between release rates towards both directions.

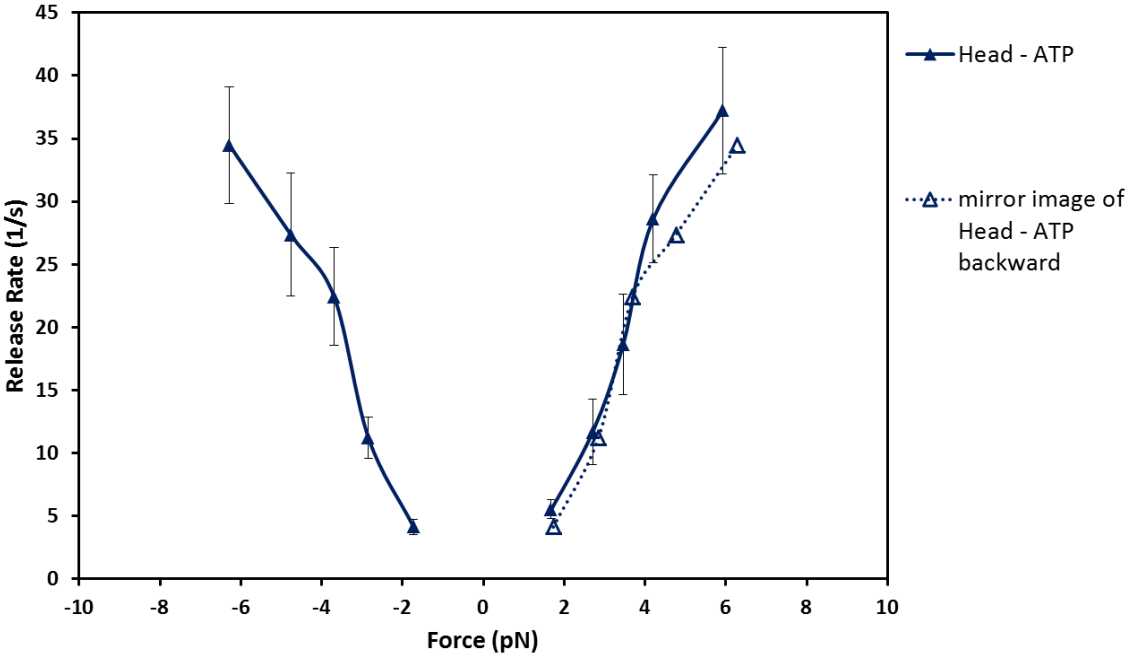

Figure 3.7. Addition of ATP increases the release towards both directions.
ATP present in the solution increases release rate of kinesin from the microtubule towards both directions.

3.2.2. Results for neck linker-pulled kinesin monomer

Figure 3.8 shows that, as for the head-pulled kinesin case, the apo release rates are low and ATP release rates are considerably higher for the linker-pulled kinesin. Interestingly, the ADP response is different from ATP in both directions and shows a clear asymmetry. This is indicative of a front head gating mechanism where ADP binding by the front head is reduced and hydrolysis in the rear head is not affected by the tension on the linker, or by its orientation.

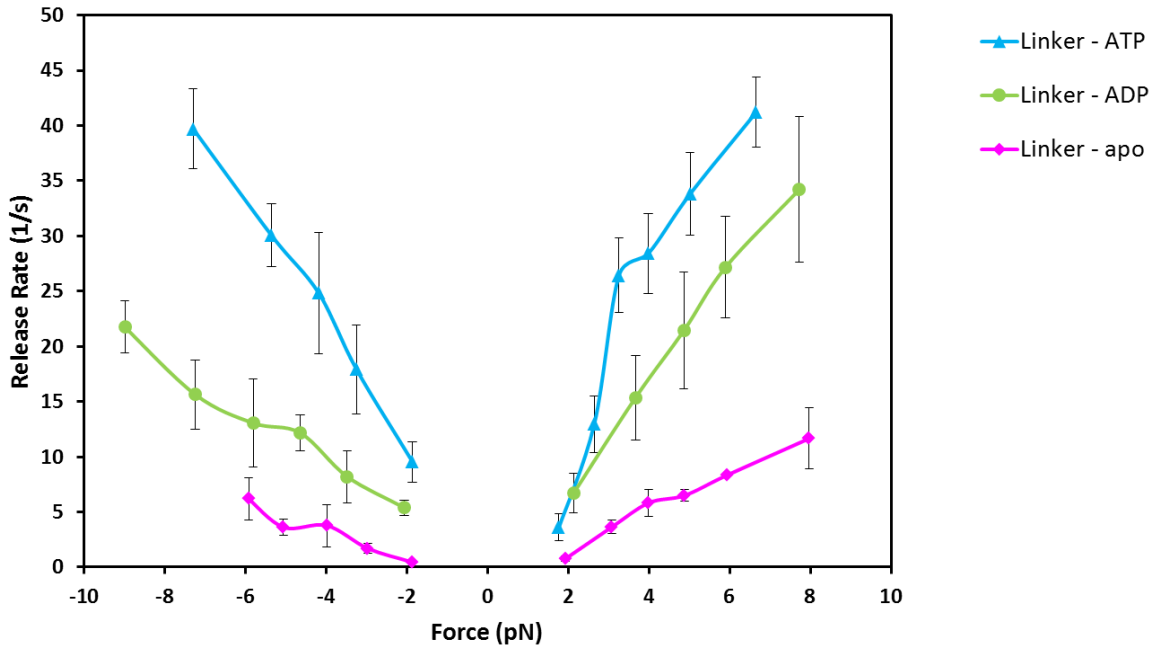

Figure 3.8. Nucleotide induced load responses of the neck linker-pulled kinesin monomer construct
Release rates under different nucleotide conditions are shown for neck linker pulled construct (Linker), where ATP, ADP and apo conditions are plotted light blue, light green and pink respectively.

3.2.2.1. Directional preference for release

Using the same reasoning for the linker-pulled monomer, if we compare backward and forward release rates under apo conditions, we see that there is a slight asymmetry between the rates (Figure 3.9). This suggests that linker orientation and pulling on the linker introduces a tendency for release in the forward direction.

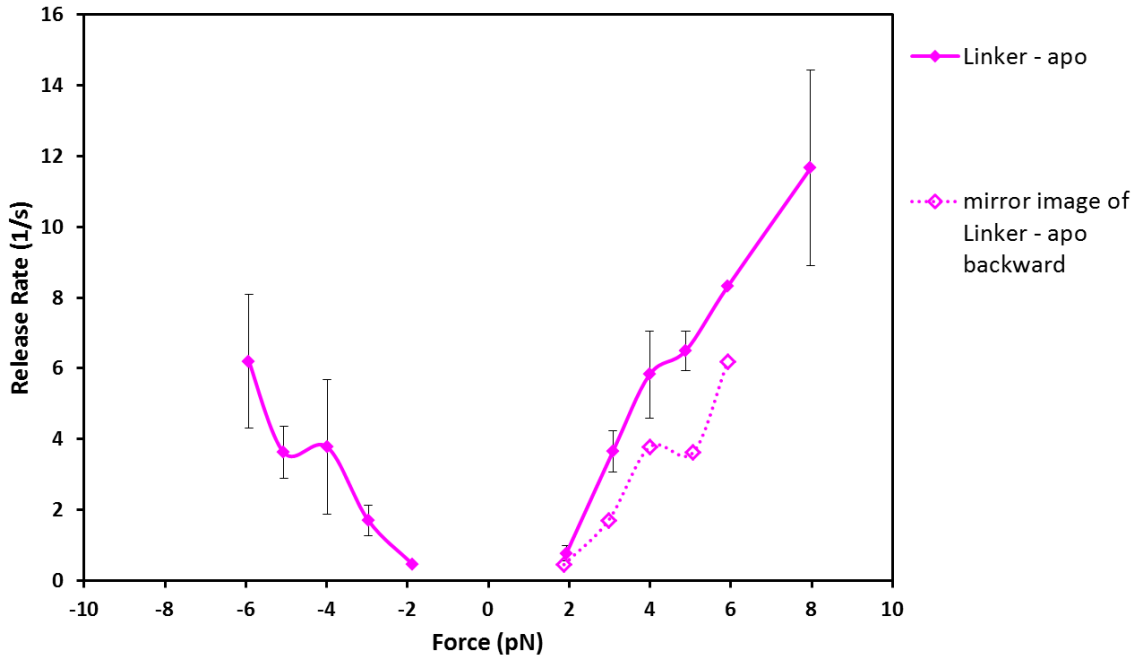

Figure 3.9. Asymmetry in microtubule release rates for linker-pulled kinesin monomer under apo conditions
Under apo conditions, mirror image of the backward release rate plot is slightly lower than the forward release rate plot suggesting a directional preference.

3.2.3. Comparison of ATP and apo conditions

Comparing the results for ATP and apo conditions for both constructs as in Figure 3.10 helps to identify any possible differences between the two constructs that may arise due to the region of pulling and have to be incorporated into the analysis. Here, the data overlaps accurately for ATP conditions and for forward release in apo conditions. This suggests that the force responses are not affected by the region of pulling.

The backward release rate for apo conditions however has decreased upon linker-pulling, which implies a structural change that contributes to a disinclination to release in the backward direction.

The accuracy of the overlap of ATP results of both constructs, in contrast to the differences in apo conditions, proves that hydrolysis is not affected by the linker, and is the dominant factor for monomer release.

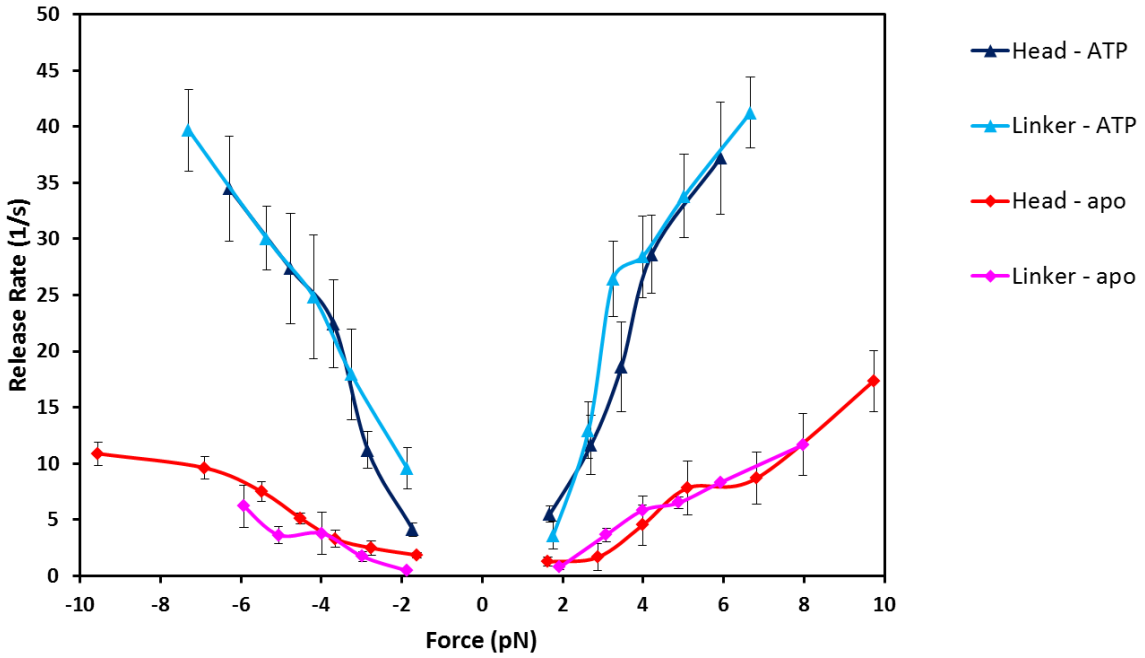

Figure 3.10. Comparison of ATP and apo conditions of both constructs
Load responses of both constructs overlap nicely for ATP and forward apo conditions. There is a slight decrease in the release rate for backwards apo conditions.

3.2.4. Comparison of ADP induced force responses

Figure 3.11 shows the ADP induced force release rates for both constructs including the mirror images of backwards release rates. Comparison of these cases makes it clear that the backwards release rate under ADP conditions are much lower for linker-pulled monomer than for head pulled monomer. Even though there is a small decrease in the release rate in forward direction as well, it is not as significant. This result proves that the orientation of the neck linker inhibits nucleotide binding to the forward head of a microtubule bound kinesin and that a front head gating mechanism is in place.

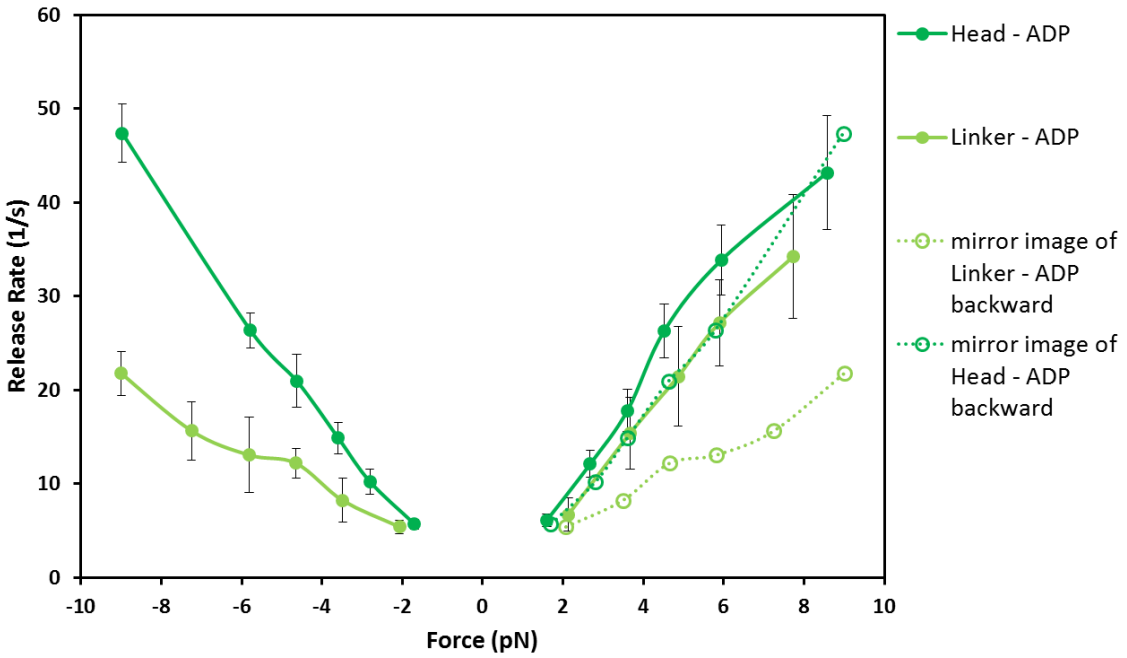

Figure 3.11. Comparison of ADP induced force responses of both constructs
Plots are shown for ADP induced release rates for both constructs including the mirror images of backward release for easy comparison. It is clear from this plot that the release rate decreases significantly when the linker is being pulled backwards.

3.2.5. Estimating the degree of gating

To determine the degree to which the neck linker orientation acts as a gate on the nucleotide binding, we have subtracted the corresponding apo responses of the head pulled monomer from each ADP curve and plotted the results as seen in Figure 3.12. These curves have been linearly fitted (dotted lines), which serves as a visual guideline to estimate the extent of gating. Assigning a 100% binding ability to forward release curve of the head pulled construct, forward release curve of the linker pulled construct maintains about 80% of this ability whereas gating reduces this to about 30% for the backwards release of the linker pulled construct (Table 3.1).

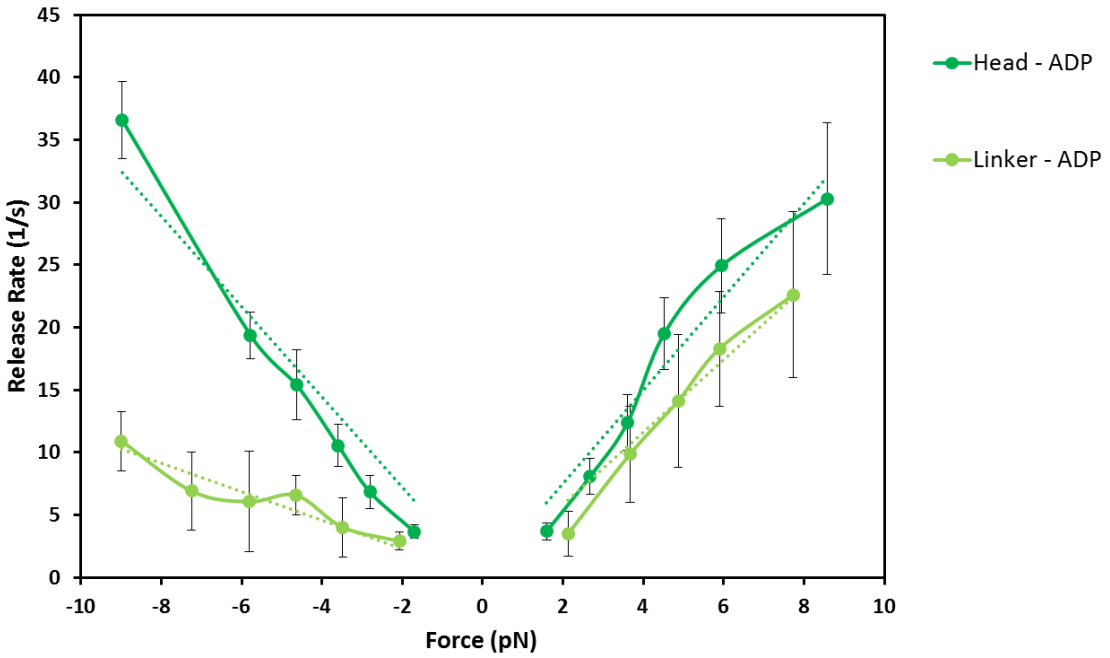

Figure 3.12. Estimation of the degree of gating
These graphs represent ADP responses after the apo responses have been subtracted. Dotted lines are the linear fits to these graphs and their slopes are used in the estimation of the degree of gating.

	Linear Fit	**Gating parameter**
Head – forward	y = 3.7406 x	100 %
Head – backward	y = 2.9202 x	96.6 %
Linker – forward	y = 3.6132 x	78 %
Linker – backward	y = 1.1401 x	30.5 %

Table 3.1. Gating parameter
Slopes to the linear fits in Figure 3.12 have been used to calculate the gating parameter where the forward pulled head-bound construct was assigned as 100% gating.

3.3. Conclusions

Based on our results, we make the following conclusions.

Hydrolysis and ADP binding are the dominant factors for microtubule release.

Release rates in both directions increase significantly in the presence of nucleotides, meaning that ATP hydrolysis and ADP binding are the primary causes for microtubule release of the optically trapped monomers. This is consistent with the results from Uemura et al. [1] where they have observed that larger rupture forces are required to detach monomers from microtubule in the strongly bound apo and AMP-PNP conditions compared to weakly bound ADP conditions (Figure 3.13).

Release rates increase with force.

As expected, release rates are higher for increasing forces in the absence of nucleotides. Remarkably, the release rates also increase as a function of force, as opposed to staying constant, for the saturating nucleotide concentrations. It is possible that the release rates under these nucleotide conditions are also force-dependent.

The linker-pulled construct data shows that there is slight asymmetry in the microtubule binding domain between the front and rear heads of a kinesin.

For linker-pulled monomer case, we observe a slight asymmetry in release rates in the presence of ATP and no nucleotides, and a significant asymmetry in the presence of ADP. Similar to our observations, Uemura, et al. [1] also report that the unbinding force is always smaller in the forward direction regardless of nucleotide state (Figure 3.13). Our assays provided more direct and detailed information about the release of monomers under different solution and pulling conditions. We directly showed that backward orientation of the linker inhibit nucleotide induced release rate, which allows us to make precise statements about kinesin gating mechanism.

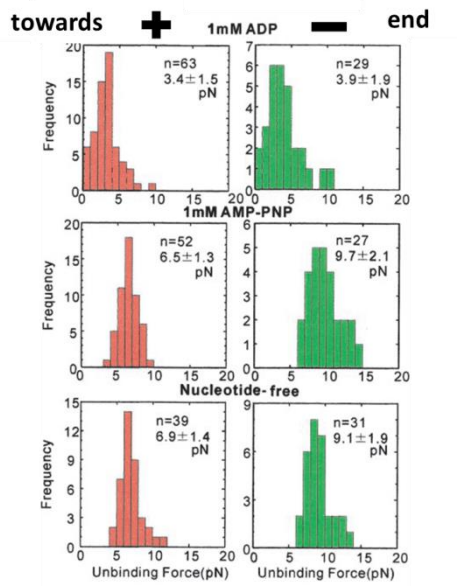

Figure 3.13. Results from relevant experiments.
Results from Uemura et al. [1] show frequency of rupture vs rupture force in different nucleotide conditions. They always observe smaller average rupture forces in the forward direction.

Nucleotide release is not affected by the linker orientation.

The results of ATP conditions prove that forcing the orientation of neck linker in any direction does not influence the release behavior. This is important especially in the case of forward pulling of the neck linker that mimics the rear head. According to our hypothesis based on the rear head gating models, we would expect an increase in nucleotide release with linker orientation if there is an assistive gating mechanism. Since we did not make such observation, we conclude that our results are not compatible with the rear head gating model.

Linker orientation inhibits nucleotide binding of the front head.

Results of ADP experiments prove that if the neck linker is orientated backwards, such as to mimic the front head, ADP binding will be inhibited. This strongly supports that kinesin stepping is coordinated by a front head gating mechanism based on the neck linker orientation.

3.4. References

[1] S. Uemura, K. Kawaguchi, J. Yajima, M. Edamatsu, Y. Y. Toyoshima, and S. Ishiwata, "Kinesin–microtubule binding depends on both nucleotide state and loading direction," *Proc. Natl. Acad. Sci.*, vol. 99, no. 9, pp. 5977–5981, Apr. 2002.

Chapter 4. Front Head Gating Model

Our results indicate that there is a front head gating mechanism regulated by the neck linker. We control the orientation of the neck linker by exerting tension, as tension and orientation are mutually dependent on each other. We prefer to attribute gating to the orientation instead of tension, based on previous studies that investigated tension in the neck linker. Yildiz et al. [1] for example have shown that lowering the tension in the neck linker does not hinder walking, but only slows it down. Similarly, Clancy et. al. [2] propose that the orientation of the neck linker (and not the tension) is responsible for gating based on their experiments with kinesins with extended linkers, where they still observe gating with reduced tension. This is also in agreement with Toprak et al.'s [3] results stating that for gating of ATP binding by the front head, neck-linkers need to be separated but it is not necessary for both heads to strongly bind the microtubule. In this case, too, the tension may be relieved from the linker of the front head, but its orientation would remain backwards and gate nucleotide binding.

The model we propose suggests that the ATP binding to the front head is gated by the orientation of the neck linker. We illustrate our model in Figure 4.1, where the initial state is two heads attached to the microtubule with ATP bound on the rear head and no nucleotide present in the front head. In this configuration, the backwards orientation of the neck linker prevents ATP binding to the front head. In state 2, ATP is hydrolyzed such that Pi is released and the rear head is left with an ADP. In this transitional state, the linker of the front head is still oriented backwards and ATP binding cannot occur in the front head. The third state is unstable weakly-interacting ADP state, where the rear head detaches from the microtubule, releasing the tension and geometrical constraints on both linkers. The front head binds ATP after the removal of the gate. Upon ATP binding, neck linker docks forward and thrusts the rear head to the front. Once the thrown head binds the microtubule, kinesin attains its initial configuration.

Our model agrees with a previous model that arised from using non-hydrolyzable nucleotide analogs to look at the gating mechanism and found that the ATP analog could only be released from the front head [4]. If an ATP was bound to the rear head, kinesin was forced to take a backwards step to release the ATP from the new front head. The model that comes from this study proposes a front head gating mechanism induced by strain. Their results however do not contradict with our gating model where binding is regulated by neck linker orientation instead.

Our study stands out as the first one that directly demonstrated regulatory role of the neck-linker orientation in nucleotide binding to the kinesin motor domain.

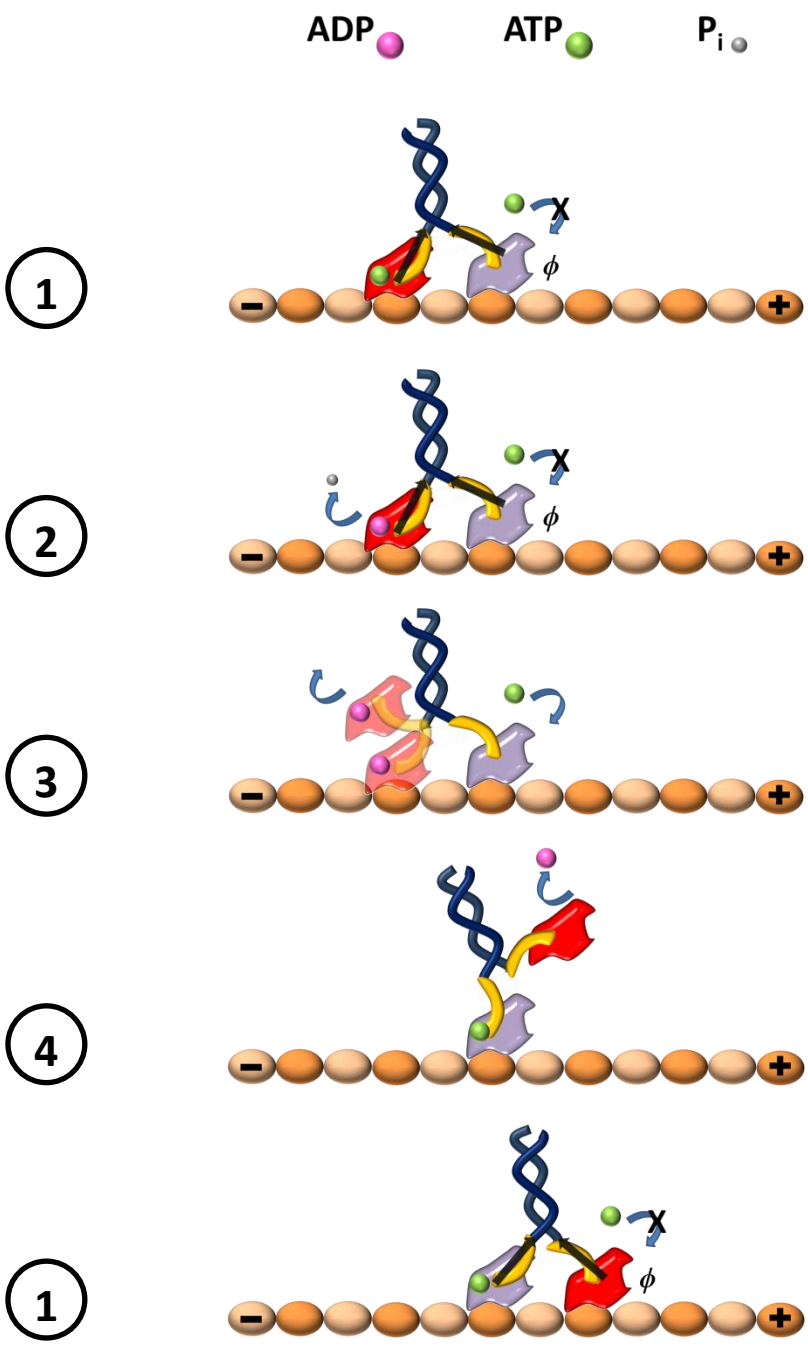

Figure 4.1. Model for gating by neck linker orientation.
1) Both heads are attached to the microtubule where the rear head has an ATP and front head is in apo state. The backwards orientation of the neck linker prevents ATP binding to the front head. **2)** Rear head has an ADP after ATP hydrolysis and Pi release. Front head linker is still oriented backwards and ATP binding is blocked. **3)** The rear head is in an unstable ADP state, where it detaches from the microtubule lifting the tension on both linkers. The neck linker of the front head can now rotate freely and the front head can bind ATP. **4)** Once the front head binds ATP, its neck linker docks forward and thrusts the other head forward. Once both heads are bound to the microtubule, kinesin returns to its initial configuration.

4.1. Conclusion

The high processivity of kinesin is remarkable among molecular motors, and attests the existence of an effective coordination scheme between its two heads. For such coordination to take place there needs to be an asymmetry in the motor that regulates the order in the stepping cycle. Many possibilities have been investigated to identify the sources of the asymmetry and how they affect kinesin stepping behavior. Based on the findings of the extensive literature, and on our current experiments, we were able to prove the source of the regulation as the neck linker orientation of the front head. When kinesin is bound on the microtubule, both heads are pointing in the same direction, but their neck linkers are in different configurations resulting in an asymmetry in the system. In the front head the neck linker is pointing backwards, and in the rear head it is pointing forward. By controlling the orientations of the neck linkers of kinesin monomers in an optical trap assay, we were able to mimic the neck-inker orientation of the front and rear heads and have shown that the neck linker orientation does not affect the nucleotide in the rear head, but inhibits nucleotide binding to the front head. Building on our findings and previous models, we were able to propose a kinesin stepping model that explains the neck linker gating mechanism.

4.2. References

[1] A. Yildiz, M. Tomishige, A. Gennerich, and R. D. Vale, “Intramolecular Strain Coordinates Kinesin Stepping Behavior along Microtubules,” *Cell*, vol. 134, no. 6, pp. 1030–1041, Sep. 2008.

[2] B. E. Clancy, W. M. Behnke-Parks, J. O. L. Andreasson, S. S. Rosenfeld, and S. M. Block, “A universal pathway for kinesin stepping,” *Nat. Struct. Mol. Biol.*, vol. 18, no. 9, pp. 1020–1027, Sep. 2011.

[3] E. Toprak, A. Yildiz, M. T. Hoffman, S. S. Rosenfeld, and P. R. Selvin, “Why kinesin is so processive,” *Proc. Natl. Acad. Sci.*, vol. 106, no. 31, pp. 12717–12722, Aug. 2009.

[4] N. R. Guydosh and S. M. Block, “Backsteps induced by nucleotide analogs suggest the front head of kinesin is gated by strain,” *Proc. Natl. Acad. Sci.*, vol. 103, no. 21, pp. 8054–8059, May 2006.